Title
Improved Resource Allocation Mechanisms in Heterogeneous Mobile Data Networks

Author
Monajemi, Pooya

Publication Date
2012

Peer reviewed|Thesis/dissertation

University of California

Los Angeles

Improved Resource Allocation Mechanisms in Heterogeneous Mobile Data Networks

A dissertation submitted in partial satisfaction

of the requirements for the degree

Doctor of Philosophy in Electrical Engineering

by

Pooya Monajemi

2013

Abstract of the Dissertation

Improved Resource Allocation Mechanisms in Heterogeneous Mobile Data Networks

by

Pooya Monajemi

Doctor of Philosophy in Electrical Engineering

University of California, Los Angeles, 2013

Professor John D. Villasenor, Chair

Femtocells, also sometimes referred to using the term "Home NodeB" (HNB), are low-power, low-cost cellular base stations utilizing a high speed internet connection as the backhaul. The recent hike in interest for femtocells in the market calls for a study of their impact on quality of service and possible mechanisms in resource allocation devised to address the problems that arise from their deployment.

The work presented concentrates on three aspects of the resource allocation problem. Firstly, the access policies in heterogeneous networks consisting of macro and femto base stations are considered with the aim to ensure acceptable quality of service provided to all users while improving for some including the owners of the device. Access policies are studied that lie between the two extremes of fully open access and fully closed to exclusive owners of the device.

The second aspect under study is packet scheduling mechanisms. While works exist on intra-cellular scheduling mechanisms as well as centralized inter-cellular schemes that provide a globally near- optimal scheduling, the body of work on global and uncoordinated scheduling mechanism is small, which is explored in this work.

The third part of the study focuses on hand-off minimization over a network

of moving mobile stations. We aim to find optimal handoff sequences in a series of predicted possible paths in front of a moving mobile station. A graph-based algorithm is explored in the third part of the study.

The dissertation of Pooya Monajemi is approved.

Mario Gerla

Lieven Vandenberghe

Izhak Rubin

John D. Villasenor, Committee Chair

University of California, Los Angeles

2013

To my parents

Table of Contents

List of Figures

List of Tables

Acknowledgments

The author wishes hereby to thank every individual who assisted in completing this work. Special thanks goes to my advisor Professor John D. Villasenor, without whose efforts and guidance this work would have been unachievable. I also wish to greatly thank the PhD committee members Professors Rubin, Vandenberghe, and Gerla for their help and attention to the project. My great appreciation goes to my colleagues at UCLA's image communications laboratory who participated in the collaborative projects that are presented in this dissertation including Dr. David Chen, Dr. Shaunak Joshi, Dr. Jianwen Chen, and Mr. Julio Navarro Lara.

Vita

2006	B.Sc in Electrical Engineering, University of California, Irvine
2008	M.Sc in Electrical Engineering, University of California, Los Angeles

Publications

David Choi, Pooya Monajemi, Shinjae Kang, and John Villasenor, *Dealing with Loud Neighbors: The Benefits and Tradeoffs of Adaptive Femtocell Access*, Proceedings of Globecom 2008

Shaunak Joshi, Ray C.C. Cheung, Pooya Monajemi, and John Villasenor, *Traffic-based Study of Femtocell Access Policy Impacts on HSPA Service Quality*, Proceedings of Globecom 2009, Dec. 2009

Pooya Monajemi, Shaunak Joshi, and John Villasenor, *Augmented Simulated Annealing for Multi-BS Block Scheduling in Heterogeneous Cellular Networks*, Submitted to the Proceedings of Globecom 2011, Mar. 2011

CHAPTER 1

Introduction

Allocation of time, frequency, and code has consistently been an important part of any cellular network design and implementation. With the advent of newer devices such as femtocells, relays, and repeaters into the cellular field, the problem of resource allocation has intensified in both complexity as well as criticality. The homogeneity of a network consisting only of standard macro base stations and user equipments (UE's, also referred to as mobile stations) is no longer a given, and any feasible resource allocation scheme must address the complexities, limitations, and opportunities introduced by the devices described above. In this work we aim to study the behavior of the heterogeneous cellular systems in addition to designing improved resources allocation mechanisms for such networks.

Femtocells, which are also sometimes referred to using the term "Home NodeB" (HNB), are the main focus of this study of heterogeneous networks due to their more complex nature. These low-power, low-cost cellular base stations are designed to serve a very small area, such as a home or office environment. There are a number of economic factors that argue strongly in favor of femtocells, including the capacity improvements that are enabled by allowing mobile stations to transmit at very low power to a femtocell that in turn utilizes a high speed internet connection as the backhaul. There is high interest in femtocells among carriers, equipment manufacturers, and other participants in the cellular industry, and many analysts expect that femtocells will significantly impact the cellular landscape over the next several years.

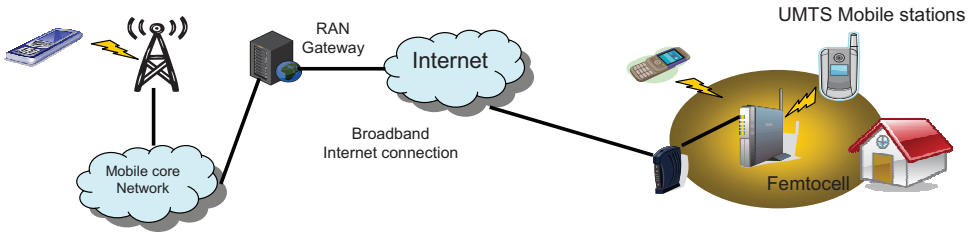

Figure 1.1: A heterogeneous network consisting of macrocells and femtocells

The work presented concentrates on three aspects of the resource allocation problem. Firstly, the access policies in heterogeneous networks consisting of macro and femto base stations will determine how the UE-BS associations will be decided. Any desirable access policy needs to ensure acceptable quality of service provided to all users while improving the service to a portion who have a better opportunity to take advantage of the femtocell base stations, as well as the owners of the device who compromise internet bandwidth. A correct design of the access policy scheme is a crucial step in the implementation of femtocells, where it can make all the difference between economic feasibility and failure of such implementations. In the work access policies are studied that lie between the two extremes of fully open access and fully closed to exclusive owners of the device.

The second aspect under study will be packet scheduling mechanisms, where the successful transmission and reception of individual packets, as well as achieving higher data rates are sought through managing the timing of users being served in each cell. A great body of works exists on localized scheduling mechanisms that work within a cell, as well as global schemes that provide a globally near- optimal scheduling using centralized decision making. Femtocell networks however suffer from a relatively slow and delayed connection to the provider's networks that makes such coordination attempts difficult to achieve. Therefore a need for a global and uncoordinated scheduling mechanism is felt, which is explored in this work.

The third part of the study focuses on hand-off minimization over a network of moving mobile stations that can be associated to either femto-cells or macro-base stations. Considering the heavy cost of a handoff (which in case of CDMA networks can only be a hard handoff) it is undesirable for a moving mobile station to associate with a local femtocell that can only momentarily provide service. Therefore we aim to find optimal handoff sequences in a series of predicted possible paths in front of a moving mobile station. A graph-based algorithm is explored in the third part of the study.

In the chapters that follow, simulation tool development has been discussed in Ch. 2, a study of femtocell access policies has been presented in Ch. 3, scheduling has been explored in Ch. 4, and handoff is presented in Ch. 5 . Conclusions and future prospects are presented in Ch. 6.

CHAPTER 2

Simulation

2.1 Introduction

An essential part of this work a on resource allocation, while not the core part, is development of effective, realistic, and precise simulation tools that can be used in understanding the behavior of complex cellular environments including macro and femtocells, and supporting a mix of circuit-switched legacy voice traffic. While we do not intend to simulate every minute detail of the communication systems under study, a level of accuracy is required in order for the study to be of interest to any entity that is part of the decision making process for the upcoming protocols. This level of accuracy has meant that while we do not simulate the physical layer signaling in detail and simulate at the "system level", we do attempt to use realistic models for information sources, link loss, transmit powers, etc.

The systems under study are in two categories. In particular, both the CDMA-based 3G system and the OFDMA-based 4G LTE systems are of interest. Two different simulation platforms are developed to study each. Realism, modular design, flexibility, and computational feasibility have been considered. The latter goal has meant that the tools were developed in C/C++ rather than Matlab in order to improve the simulation speeds. In the following sections the 3G and the 4G simulation tools are described separately.

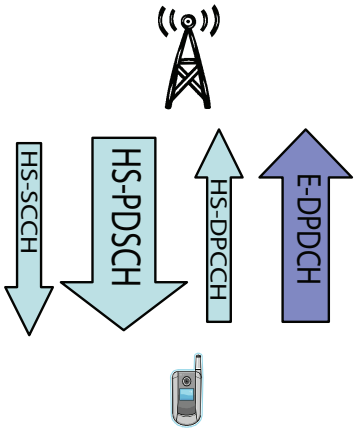

Figure 2.1: The HSDPA High speed downlink control, high speed downlink data, and high speed uplink control, and the HSUPA high speed uplink data channels

2.2 WCDMA-HSPA Simulation

Proper modeling of the HSPA channels requires a dynamic simulator in which the network behavior is evolved over a series of time slots. The simulation environment utilized in the work performed here has been constructed by starting with a static simulator for legacy WCDMA circuit-switched voice communications developed by Laiho and Wacker [LW01]. In this simulator a set of iterative downlink and uplink computations are performed that simulate the feedback power control schemes in effect in the WCDMA system. Convergence of the computations to a stable condition then provides a near-optimal solution to the transmit powers in the interference-limited CDMA system.

Building on top of this tool, a dynamic simulator was created to enable handling of packet data. The changes included 1) the addition of mechanisms to handle the high speed downlink control, uplink control, and downlink data channels for HSDPA and high speed uplink data for HSUPA (see Fig. 2.1), and 2) the addition of the time slotted structure and scheduling methods to introduce

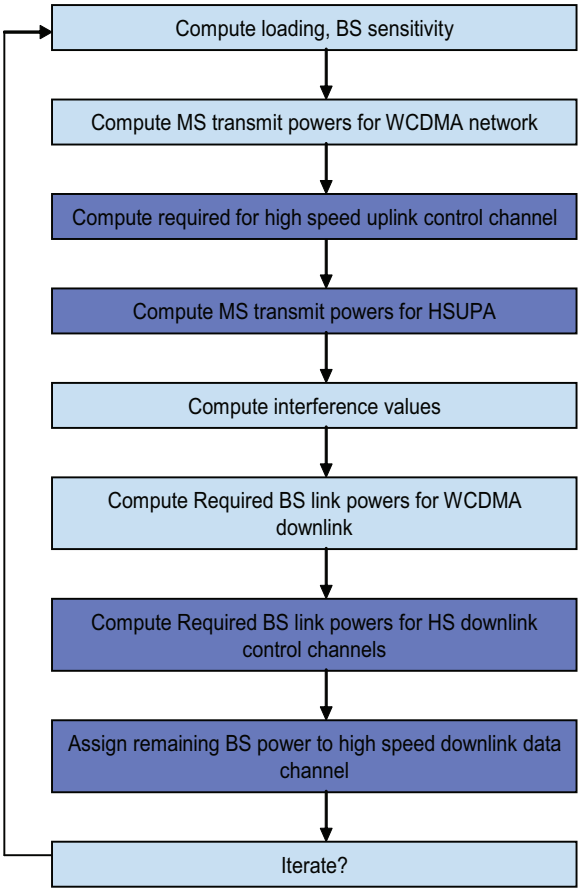

Figure 2.2: Computations performed in each iteration of the augmented simulation

dynamism.

The addition of high speed channels into the iterative sets of equations resulted in the flow shown in Fig. 2.2.

2.2.1 High Speed Downlink Control Channel

The high speed downlink control channel (HS-SCCH) uses a downlink data rate of 18.5 kbps in accordance with [Speb]. The E_b/N_0 requirement of this channel is set to be 12 dB. The computed power in the base station is compared to the link power limitation (as is done in the legacy channel model) to check for base station link outages. It is also summed with legacy powers to find the total base

station power. This quantity is compared with the maximum total base station power limitation to identify potential outages and is subsequently used in the computation of interference levels.

2.2.2 High Speed Uplink Control Channel

The high speed uplink control channel (HS-DPCCH) is used to transmit acknowledgements (ACK) and channel quality indicator (CQI) information during the first 0.67 msec and remaining 1.33 msec of each 2 msec subframe respectively. The uplink data rate is 15 kbps for both the ACK and the CQI. The E_b/N_0 requirement of the channel during ACK is estimated from [Spea] to be 6.9 dB for a 1% error rate, and the E_b/N_0 requirement of the channel during CQI is set to 3.9 dB. The computed power in the mobile station is added to the legacy channel powers and compared to the maximum mobile station transmit power limitation.

2.2.3 Modeling the High Speed Downlink Data Channel

The high speed downlink data channel (HS-PDSCH) differs from conventional WCDMA channels in that it utilizes adaptive modulation and coding (AMC) as opposed to the power control mechanisms. Instead of computing an optimum power level, the base station maximizes the transmission data rate for a given HS-PDSCH channel power level by selecting an appropriate modulation scheme (QPSK vs. 16-QAM), coding rate, and number of multicode channels utilized (out of 15 total) based on the available power, link loss data, and interference at the receivers.

There are many possible design choices regarding how many high speed downlink data channels are used at one time. These choices involve a large number of tradeoffs, some obvious, and others much less so, that impact the overall effectiveness of the high speed data delivery. In [BBR99], it has been proposed that

the optimal number of mobile stations per time interval is one, and that is the approach that has been used in the experimental results presented here, though this is obviously an area of interest for further exploration.

The HS-PDSCH channel power is modeled as a power assignment in the base station. This power level is chosen as the lower of the available base station power and 30% of the total base station power. Adaptive Modulation and Coding (AMC) is then used to calculate the optimal high speed downlink bit rate.

2.2.4 Modeling the High Speed Uplink Data Channel

In HSUPA transmissions, power is allocated to the high speed uplink data channel (E-DPDCH) using a loading-aware approach based on the current load on the base station serving the UE in question. The amount of additional UE transmit power that would be required to overload the base station at the time slot in question is determined. After allowing 3dB of headroom, a certain amount of power is allocated to E-DPDCH (only if the UE is able to fulfill this power allocation without surpassing its own overall transmit power limitation). If the UE is not able to meet the allocated transmit power, a fraction of the difference between maximum UE transmit power capability and target power allocation is used. Scheduling is coordinated so that one UE is sending uplink data at a time to any given base station. The instantaneous uplink data rate calculation is based on the received signal-to-interference-noise ratio (SINR) at the serving base station.

2.2.5 Time Slotted Simulator Implementation for HSPA

Here we mainly focus on the HSDPA aspects of the time slotted simulation. Similar concepts can be extended to the HSUPA, however they were not implemented in the simulation tool for HSUPA in the same level of detail since we are mostly interested in the uplink control channels and the downlink control channels would

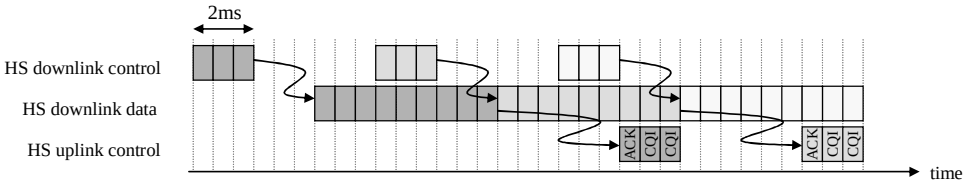

Figure 2.3: High speed downlink control, high speed downlink data, and high speed uplink control channel timing for the time slotted simulator implementation (HSDPA)

not be very relevant to the performance.

The high speed downlink control, uplink control, and downlink data channels are active during different stages of high speed transmission. High speed downlink control information, which is necessary for signaling the transport format and the multicode information used for decoding high speed downlink data, is sent first. Downlink data then arrives through the high speed downlink data channel. After data has been received and processed, the mobile station sends ACK and CQI messages that are then used by the base station for the next transmission.

Time is considered in 667 μsec slots and each of the three channels is either included or excluded from calculations in each time slot. Each time slot is independently simulated using the augmented static simulator to identify the optimum power levels at each point in time. The downlink control signals are sent in the first 3 slots, the high speed downlink packet is sent in 9 slots, the uplink ACK utilizes 1 slot, and the uplink CQI data spans 2 slots (Fig. 2.3). The time between high speed downlink control and high speed downlink data is set to be 3 slots to allow the mobile station to process the downlink control data, and the time between receiving the high speed downlink data and sending the high speed uplink control is set to be 6 slots to allow for propagation delay and processing on the mobile station.

A scheduler performs the task of choosing the high speed users at each base

station for each packet, and determines the channels that are active for each slot. To reflect the assignment of multicodes to exactly one mobile station at a time, only one mobile station can be the high speed user per base station. For the simulation, a round robin scheduler is used wherein all mobile stations connected to a given base station that desire high speed downlink data take turns being the high speed user. In order to avoid synchronous transmission of ACK signals in all base stations, a random offset of between 0 and 8 time slots is introduced at each base station. All users are assumed to have voice channels active at all times and to be always ready for receiving high speed data. They are also assumed to be capable of receiving and processing all available AMC combinations and any number of multicodes (up to 15).

For the results described here, the simulation duration spans 3000 time slots, which is equivalent to 2 seconds. During this period mobile stations are assumed to have constant link loss. A given high speed packet transmission is classified as a failure when the mobile station is put to outage in any of the time slots except CQI.

2.3 OFDMA-4GLTE Simulation

Due to the differences between the physical layers of the LTE systems and the WCDMA systems, it was necessary to develop a completely new simulation tool to address the LTE system specifications. A generic system schematic is shown in Fig. 2.4, that contains both the link-level and the system-level simulation layers. Being interested only in the system-level aspects, we use a tabulated version of a set of independent link-layer simulation results to be used in the system-level simulation phase in an abstracted manner.

The generic flow of the LTE simulation tool is shown in Fig. 2.5, where each iteration corresponds to one time slot in the scenario being simulated. Multiple

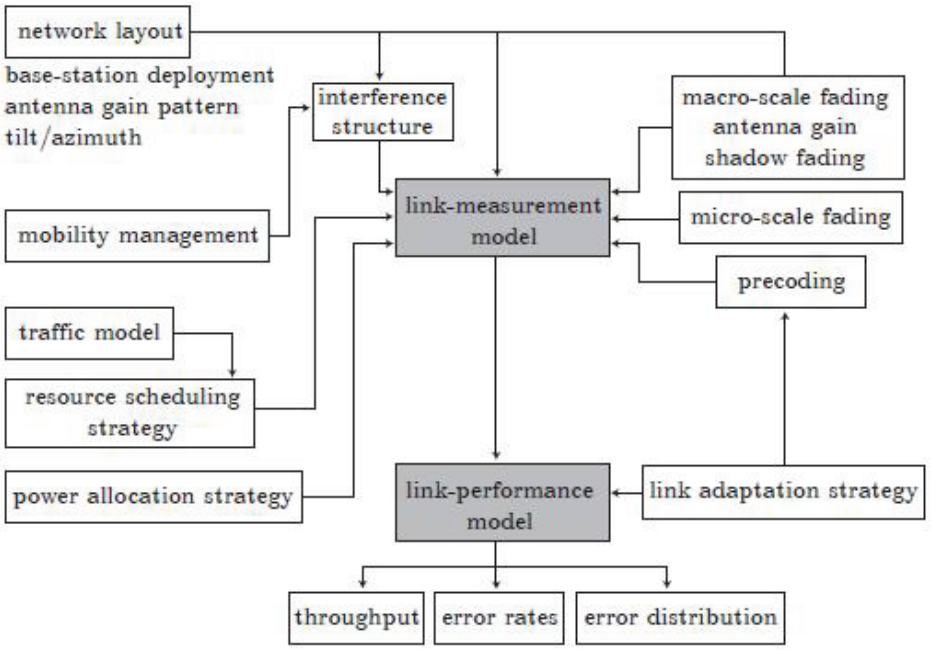

Figure 2.4: LTE simulation schematic, including both link-level and system-level

object types are present:

1. **UE** handles generation of uplink and downlink data requests, which can be performed in a full buffer manner or as a Poisson process. Data rates achievable on both uplink and downlink are also computed by the UE using one of two possible methods of Shannon channel capacity and link-level simulation table lookup. The UE also handles motion if enabled.

2. **BS** handles scheduling, which can be implemented using various schemes. Round robin, proportionally fair, and simulated annealing variants are supported (see ch. 4).

3. **RNC**, or the Radio Network Controller, handles the BS/UE associations. In the case of simulated annealing, the RNC also handles the accumulation of collision rates and signaling the decisions.

4. **Channel** simulates the OFDM channel by independently fading a set of

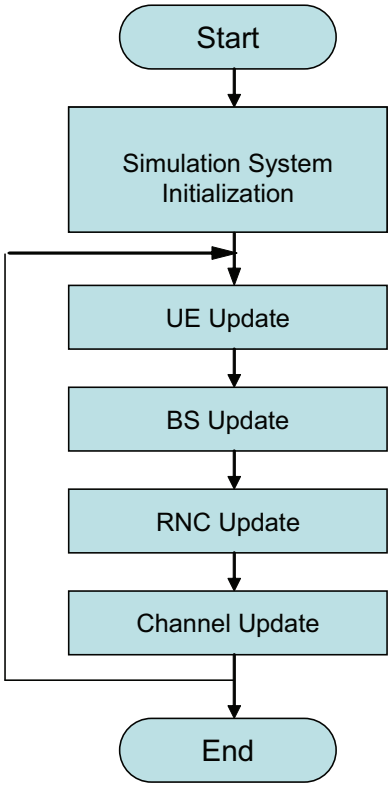

Figure 2.5: System-level LTE simulation flow chart

multiple rays with different delays and gains. Combination of these rays will provide channel gains for each subchannel frequency used in the OFDMA scheduling scheme.

For each time slot each of the objects are updated and their results made available to the rest of the entities in the simulation.

CHAPTER 3

Femtocell Access Policy

3.1 Introduction

One of the most interesting open technical questions concerns how best to optimize the performance of networks including femtocells in light of the interactions between femtocells and UEs that may be near, but not communicating with, the femtocell. Like WiFi access points, femtocells can be operated in a closed subscriber group (CSG) manner (also called "closed access"), in which only UEs with proper authorization can connect, or under an open access policy, in which UEs outside the CSG are permitted to connect to the femtocell. If an UE is very near to a femtocell but unable to connect to it, it will need to connect to a regular ("macro") base station that may be hundreds of meters away. This creates the potential for a "loud neighbor" effect, in which the strong signal from this UE contributes significantly to the noise environment in the neighborhood of the femtocell.

At the highest level, the open/closed issue is one which balances the benefits of interference reduction against the costs of femtocell resource sharing. Awareness of these issues has led to the recent introduction in the standardization process of "hybrid" femtocells [Rel], in which some portion of the femtocell resources are reserved for the exclusive use of the CSG, while the remaining resources are open.

One way to circumvent this problem is to use a separate, dedicated channel for the femtocells at a different frequency from that employed by the macro base

stations in a network. However, in many cases this will not be possible because a single carrier may not own enough spectrum. For example, in many regions carriers have licensed three 5-MHz frequency bands, and in order to maximize revenue, will fully utilize this spectrum for traditional macro cellular services. To the extent that femtocells are added in such in environment, they will have to operate in a co-channel manner, sharing the same spectrum as the macrocells and thereby creating a potential for the interference effects described above. In dense urban areas, this effect can be significant. For example, in office complexes and apartment buildings in an urban core, there can easily be several hundred people within a few tens of meters of a given location. Even after adjusting for multiple carriers, frequency bands, and the expected use patterns of individual UE users, there can easily be significant numbers of active UEs near to, and at the same frequency as, a given femtocell.

The issue of how best to manage co-channel femtocells has been given significant attention in the 3GPP industry group, with particular attention to the performance under the two scenarios of open or closed access. These studies have explored issues including downlink capacity for networks with open vs. closed access [Nor07], the effect of the number femtocells on the capacity of a macrocell [Nok07], and examinations of interference impacts involving various combinations of femtocells and macrocells [Ora07]. The conclusion from these studies is that a closed co-channel femtocell can lead to significant interference problems for all parties, particularly if the femtocell does not adaptively change its transmit power in order to minimize its interference on existing networks [TR2].

The goal of this chapter is to explore some of the subtleties involved in open access, and in particular to examine the tradeoffs associated with different levels of open access. The underlying premise of this chapter is that the value of a femtocell both to its owner and to the overall network will be maximized if the level of open access is adaptively controlled as a function of factors including the

instantaneous load on the femtocell. While a closed femtocell can be problematic as noted above, in an environment with a high density of UEs a completely open femtocell can also suffer problems, because it will potentially force the sharing of limited femtocell wireless bandwidth and internet backhaul capacity among significant numbers of UEs,with obvious detrimental consequences to the service level available to the owner of the femtocell.

The remainder of this chapter is organized as follows. We explore the impact of access policy choice in HSDPA-dominated networks in Section 3.2. Next in Section 3.3 we direct attention to the interrelationship between traffic type, access policy, and performance. Conclusions are offered in Section 3.4.

3.2 HSDPA Results

There is clearly an enormous range of scenarios that could be considered using the modeling environment described in Chapter 2.In the interest of clarity and brevity, we limit consideration here to one specific scenario that is very effective at illustrating tradeoffs in femtocell access policy.

We have considered a scenario in which we define a number of randomly distributed "indoor" and "outdoor" environments with macrocells, femtocells, mobile stations. An "indoor" environment is a circular region 20 m in diameter surrounded by walls that attenuate all signals traversing them by 15 dB. Inside each indoor environment are two indoor users. All other locations on the map are "outdoor" environments. This is shown in Fig. 3.1, which contains 32 "indoor" environments designated by circles (indoor environments that include a femtocell) and an additional 32 indoor environments designated by squares (indoor environments with no femtocell). There are also 21 macrocell base stations, designated by lines, each serving a single 120-degree sector. Finally, there are 456 mobile stations designated by dots.

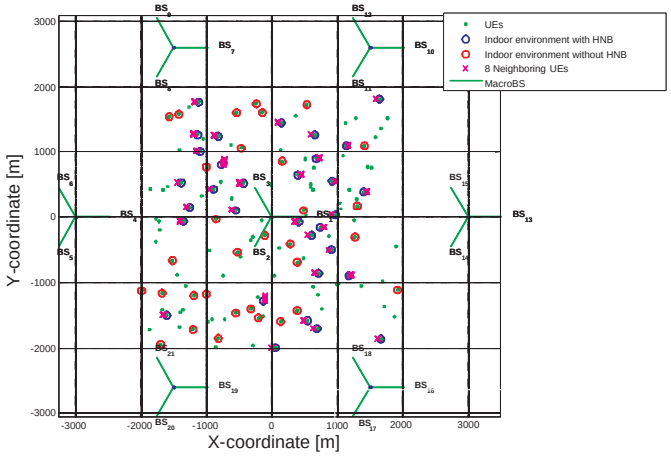

Figure 3.1: Positions of UEs, indoor environments, femtocell locations, and macro base stations.

The two users inside each femtocell are within the closed subscriber group of that femtocell, and are referred to as the "CSG UEs". In addition, there are clusters of eight UEs that are near to but outside the walls of the indoor environments containing the femtocells, and for which the common pilot channel (CPICH) signal received from the femtocell is stronger than that received from the macro base station. UEs that fall into this category are referred to as "neighbors", as they could potentially connect to the femtocell under an open access scenario.

The service results are shown in Fig. 3.2. Different positions on the horizontal axis represent different policies for femtocell access. At the left end of the axis, the case with no femtocells is considered. In this case all of the UEs, including the two UEs that will later be part of the CSG, connect (or attempt to connect) to the macro base stations. The next position on the horizontal axis is labeled 2CSG, and considers that performance when the femtocells are present and the access is closed so that only the two CSG mobiles can utilize them. As one moves further to the right on the axis, successively larger numbers of neighbors are granted access to the femtocells.

The vertical axis gives the number of UEs associated with the macro and fem-

tocell that are served and in outage. For example, when there are no femtocells, 406 of the 456 UEs receive service using the macro base station. When the femtocells are present and limited to the fully closed ("2CSG") approach, 212 UEs are served by the macro base stations and 177 UEs are not served, while 67 UEs are served by the femtocells. Thus, it can be seen that in this scenario, introducing femtocells with a closed access policy results in a decrease in service. This is due to the interference that the femtocells and the femtocell users are generating, which is sufficiently harmful to the macrocell users to cause outages. However, as the femtocell is opened up to allow more users, the overall service improves. It can be seen that allowing 6 neighbors into the femtocells results in similar service to the macrocell-only scenario, and that opening up access policy further results in even better service.

The throughput results are shown in Fig. 3.3. Just as in Fig. 3.2, different positions on the horizontal access represent different policies for femtocell access.

The vertical axis gives the average throughput for those UEs connecting to the macrocell (dark bars), the femtocell (light bars), and the average over all mobiles in the system (solid line with triangles).

Notably, in the fully closed approach, the average femtocell UE throughput is maximum at 3.17 Mbps. As the access policy is changed toward a more open policy, the average femtocell UE throughput decreases. This is because the femtocell needs to share its bandwidth among the neighbors that receive access to the femtocell. Moreover, as more users are allowed into the femtocell, the number of users served per each macrocell decreases, so the throughput enjoyed by the macrocell users increases.

The optimal operating point for this scenario is dependent on perspective. From the standpoint of the femtocell owner, a closed access policy is optimal, because all CSG UEs are successfully able to connect and their throughput is maximized. From the standpoint of those users in the system who are not using

the femtocell, a fully open approach (in which all eight neighbors are granted access) is optimal, because in this case the femtocell is providing maximal relief to the load on the macrocell, thereby enabling those UEs still using the macro base station to receive higher throughput. A limited access policy of allowing 6 neighbors into the femtocell results in similar service levels to the macrocell-only scenario, but with a significantly improved throughput.

In sum, allowing access to six neighbors maintains the same level of outage performance while improving throughput performance for all the UEs relative to a system with no femtocell or a fully closed femtocell. In the particular scenario explored in Fig. 3.1, the presence of the femtocell is a win-win - the femtocell owners benefit, as do the other UEs, even those not utilizing the femtocell. In other simulations, we have found that the choice of optimum operating point depends very strongly on the specific scenario, and in addition on the metric chosen for defining "optimum". For example, additional scenarios have shown benefits of a limited access policy at different optimal operating points, allowing 5, 6, or 7 neighboring users. More important however than the specific results for any one scenario is the general result that the performance of different access policies is highly dependent on the specifics of the scenario, and that all participants in the system have a strong incentive to make sure that access strategy is well managed.

3.3 Mixed-Traffic Results

HSDPA and HSUPA are different in many respects, and it stands to reason that access policy decisions will impact them differently. In addition, the way in which the overall network responds to access policy choices depends in part on the specific mix of traffic types on the network. To examine this, we here explore the relationship between access policy and service quality across a broader range of traffic types to determine optimal network performance (in terms of service and

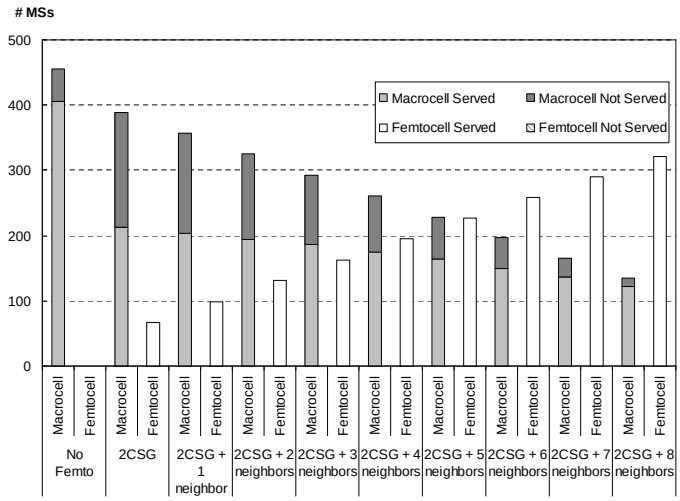

Figure 3.2: Service as a function of different femtocell access policies, ranging from no femtocell, a fully closed femtocell ("2CSG" label), and successively more open access as one moves to the right on the horizontal axis.

throughput) for a given scenario.

Fig. 3.4 provides information about the system configuration used in the experiments. Similar to the scenarios in Section 3.2, the system contains a total of 21 macro base stations located at 7 sectorized sites, 456 UEs, and 32 femtocells. There are 32 indoor environments with femtocells, with each femtocell associated with two CSG UEs also located indoors (though potentially separated from the femtocell by one or more indoor walls). In addition there are 8 neighboring UEs near each femtocell, separated from the femtocell by an indoor/outdoor transition wall, and located at a distance from the femtocell of less than 100 meters. There are also 32 indoor environments, each containing 2 UEs in which there is no femtocell present. Finally, there are 72 outdoor UEs. Signal loss through indoor and indoor/outdoor transition walls is modeled using a histogram-based wall loss model.

One of the challenges in modeling highly complex networks with hundreds of UEs lies in efficiently presenting performance data. We believe that packet success

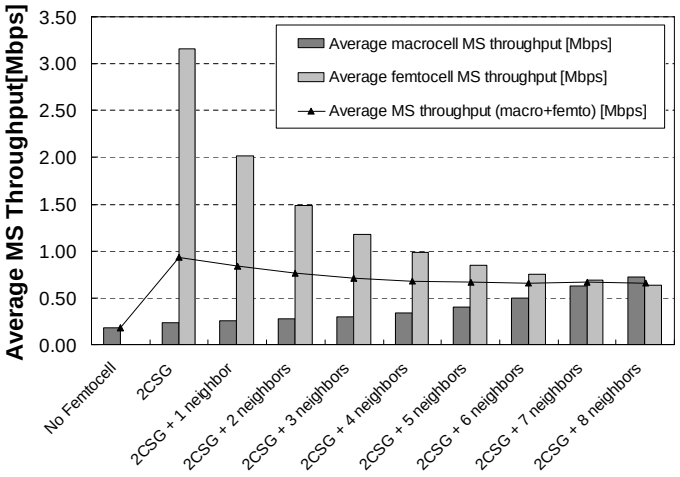

Figure 3.3: Average throughput as a function of different femtocell access policies, ranging from no femtocell (e.g. the femtocell is not present or is powered down) at the left end of the axis, a fully closed femtocell ("2CSG" label), in which only the two UEs that are members of the CSG are allowed to connect), and successively more open access as one moves to the right on the horizontal axis.

rates (PSR) are a useful metric because they directly indicate an important aspect of performance, and because they can be used to derive information about the performance of applications such as media transmissions. Fig. 3.5 shows a conceptual example of how PSR information can be conveyed in an intuitive visual fashion. This figure is a complimentary cumulative distribution function (CCDF) for the PSR, with the vertical axis indicating the fraction of UEs and the horizontal axis providing the minimum PSR rate for the associated fraction of users.Accordingly, "good" performance is exemplified by the upper curve in Fig. 3.5 which shows the curve passing through (fraction of UEs=0.9, PSR=95%), meaning that 90% of the UEs have a PSR of at least 95%. The middle curve illustrates a system with "medium" performance; in this case the passage of the curve through (fraction of UEs=0.6, PSR=50%) means that 60% of the UEs have a PSR of at least 50%, and thus conversely, that 40% of the UEs have a PSR of less than 50%. Finally, the lower curve illustrates a system with "poor performance". In this example,

Environment Type	UEs per environment	Environ-ments	Total # of UEs
Indoor environments with HNBs	2 CSG UEs	32	2*32 = 64
	8 neighboring UEs	32	32*8 = 256
Indoor environments without HNBs	2 UEs	32	32*2 = 64
Outdoor	72		72
	Total UEs:		456

Figure 3.4: System configuration.

the curve passes through fraction of UEs=0.1, PSR=5%), which means that 90% of the UEs have a PSR of below 5%.

Fig. 3.6 illustrates the PSR complimentary cumulative distribution function for UEs connected to the femtocells. Three curves are shown, corresponding respectively to a fully closed access policy (curve labeled "CSG"), an access policy in which the CSG plus four neighbors are granted access ("CSG+4"), and an access policy in which the CSG plus eight neighbors are granted access ("CSG+8"). This figure, and in particular the negative slope of the CSG and CSG+4 curves indicates a wide range of HSUPA packet success rates for UEs served by femtocells when there are other nearby UEs performing HSUPA transmissions to a macro base station and not to the femtocell. Under such a scenario, the uplink interference generated by other cells (in other words by the neighboring UEs not connected to the femtocell) changes significantly from time slot to time slot, often resulting in interference with HSUPA transmissions involving the femtocell-associated UEs. When the access is opened to allow all neighbors to utilize the femtocell (CSG+8 curve) there is a marked improvement in PSR. This is due to the reduced interference levels from other (non-femtocell) cells. Most fundamentally, when an femtocell allows a formerly excluded UE to connect to it, the femtocell can then exert scheduling control over the UE HSUPA transmissions. This benefit of allowing the femtocell to directly manage transmissions in its vicinity in many cases

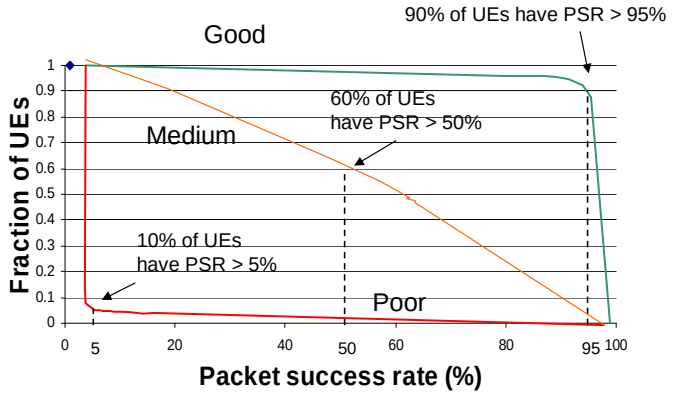

Figure 3.5: An example plot showing how packet success rate can be conveyed using a complimentary cumulative distribution function (CCDF). A point on the plot indicates that the associated fraction of UEs (vertical axis) experience a PSR of at least the value indicated by the horizontal axis. Three illustrative curves are shown. For example, the "good" illustrates a system in which 90% of the UEs experience PSRs of greater than 95%.

will be well worth the price paid in resource sharing.

Fig. 3.7 shows the PSR for UEs connected to the macro base station. Curves for the three access policy scenarios "CSG", "CSG+4", and "CSG+8" are again given, as well as a curve "no femtocell" corresponding to the case where there are no femtocells present. In contrast with the UEs connected to the femtocell in Fig. 3.6, in Fig. 3.7 there is much less improvement in the PSR as a function of femtocell access policy change. The most significant change occurs in PSR improvement in the transition from a system with no femtocells to one with femtocells, regardless of access policy. This is due to the overall reduction in interference experienced by the UEs connected to the macro base station when other UEs are "offloaded" onto the femtocell, and thus perform transmissions using lower power. It is also worth commenting on why going from CSG only to CSG+8 has a lower impact in Fig. 3.7 than in Fig. 3.6, because both macro base stations and femtocells impose scheduling control over their respective UEs. The impact is not symmetric

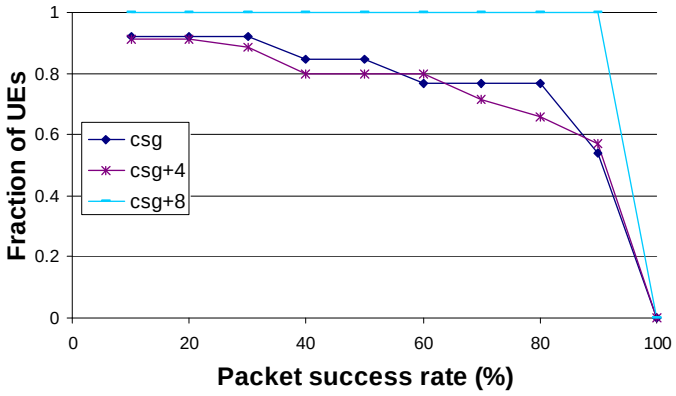

Figure 3.6: HSUPA packet success rates for UEs connected to the femtocells. Three curves are shown, corresponding to completely closed access ("CSG"), allowing the four neighboring UEs to connect ("CSG+4"), and allowing all eight neighboring UEs to connect ("CSG+8"). Performance improves significantly once all neighbors are allowed access, as this enables the femtocell to exert scheduling control over HSUPA transmissions.

because UEs associated with a femtocell transmit with much lower power than UEs associated with a macro base station. Thus, the HSUPA transmissions of femtocell UEs have a much lower impact on macro base station UEs than the other way around.

It is also important to recognize that (in both Fig. 3.7 and Fig. 3.6) the set of UEs represented by the curves expands or contracts as access policies change. Thus, for example, there are more total UEs represented by the "CSG" curve in Fig. 3.7 than by the "CSG+8" curve, since the act of opening access has moved some UEs off of the macro base station and onto the femtocell. A UE that remains connected to the macro base station across all access policies will have a proportionally larger impact on the overall packet success rates in Fig. 3.7 as the access is progressively opened. A converse effect occurs with Fig. 3.6. While these effects do not impact the specific observations above, there are scenarios and circumstances under which this is a factor, as discussed below.

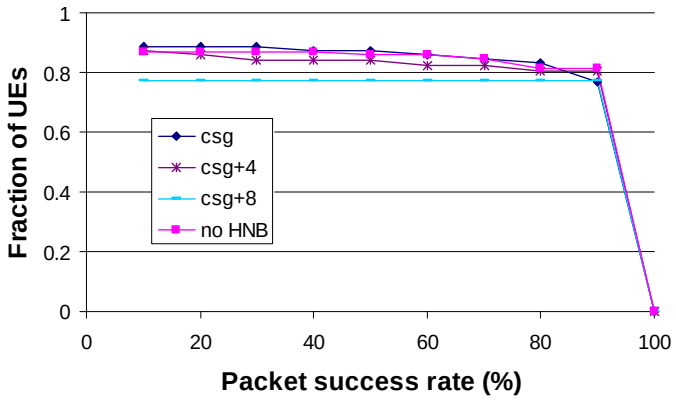

Figure 3.7: HSUPA packet success rates for UEs connected to the macro base station. Four curves are shown, corresponding to a system with no femtocells ("no femtocell"), completely closed access ("CSG"), allowing the four neighboring UEs to connect ("CSG+4"), and allowing all eight neighboring UEs to connect ("CSG+8") In contrast with the femtocell case in Fig. 3.7, the PSR for UEs connected to the macro base station shows a much less significant improvement with femtocell access policy changes, though going from "no femtocell" to any femtocell scenario does give some improvement, due to reduced interference levels.

Fig. 3.8 shows the PSR performance for HSDPA for UEs connected to the femtocell. Unsurprisingly given the proximity of the femtocells to the UEs, the PSR rates are very high regardless of access policy. In contrast with HSUPA, in which interference from macro-connected UEs impeded transmissions of femtocell-connected UEs, with HSDPA UEs connected to the macro base station do not generally cause large enough downlink out-of-cell interference to disrupt downlink transmissions from the femtocell to the UEs connected to it. This is in part due to the fact that HSDPA downlink power in a transmission from a macro base station to a UE is independent of the served UE location with respect to femtocells in the system. By contrast, the loading on the femtocell is impacted by HSUPA transmissions from nearby, macro-connected UEs.

Fig. 3.9 shows the performance for HSDPA for UEs connected to the macro

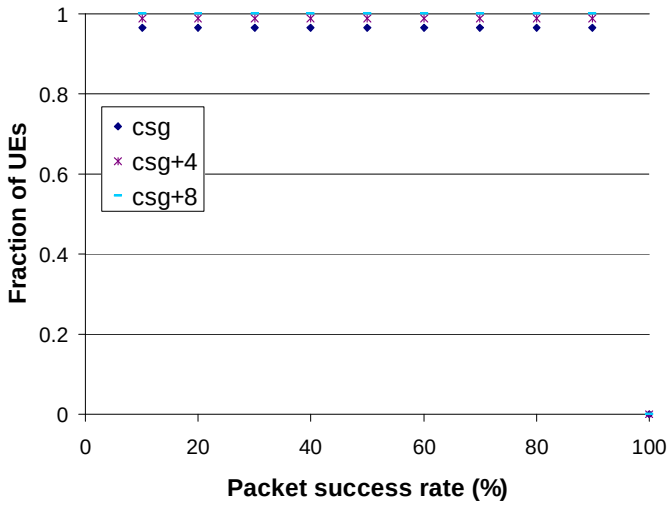

Figure 3.8: HSDPA packet success rates for UEs connected to the femtocells.

base station. One of the most notable features of this figure is the reduction in PSRs in going from a system with no femtocells to the "CSG" case. This is due to two factors. First, as discussed earlier, the system includes 32 femtocells having 8 neighbor UEs each. Thus, there are a total of 256 UEs that are very near to, but in the case of "CSG" operation, excluded from access to femtocells. When the femtocells are turned on under a "CSG" access policy, the potential gain in PSR enabled by lower transmission power of the two CSG UEs now connected to the femtocell is more than outweighed by the interference experienced by the neighbor UEs due to the femtocell transmissions. As access is opened up, more of these neighbors are connected to the femtocell, thus the fraction of overall macro base station UEs that are also non-femtocell-connected femtocell neighbors is reduced, and the overall PSRs rise. Even in the "CSG=8" case, however, when all neighbors have been admitted to the femtocells, the PSR remains lower than it was with no femtocells. This is because there are some macro-connected, non-neighbor UEs that, due to distance to the macro base station and/or location in poor propagation environments, have poor PSR regardless of femtocell access policy. These UEs constitute a higher proportion of the macro-connected UEs as

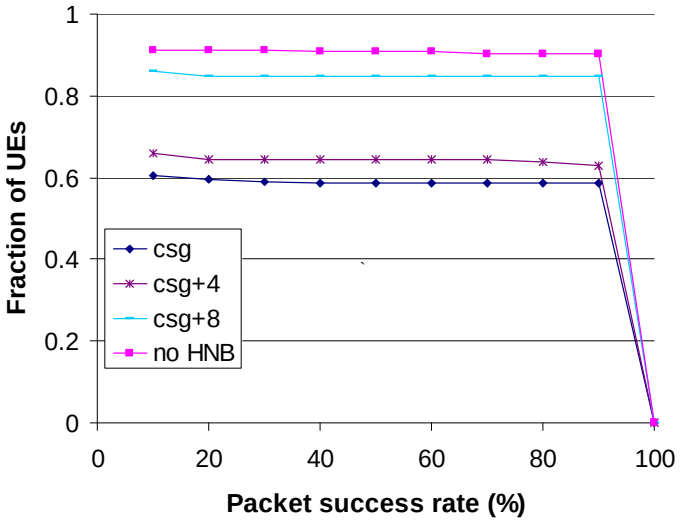

Figure 3.9: HSDPA packet success rates for UEs connected to the macro base station.

access policy is opened, and thus have a larger impact on the PSR computation.

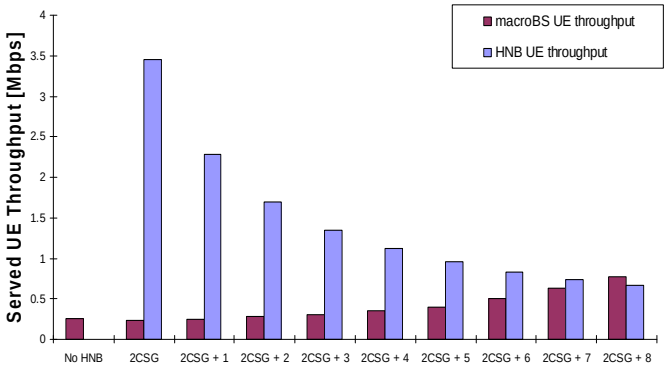

Figure 3.10: HSDPA throughput for UEs in the HSDPA-dominant scenario. The dark/red bars correspond to macro-connected UEs; the light/blue bars correspond to femtocell-connected UEs.

Figures 3.10 through 3.13 present throughput results. These figures show HSDPA and HSUPA throughputs for two different scenarios: HSDPA dominant, and HSUPA dominant. In the HSDPA dominant scenario, 90% of the UEs are engaged in HSDPA only, while the remaining 10% are simultaneously using all of HSDPA, HSUPA, and voice. In the HSUPA dominant scenario, 90% of the UEs

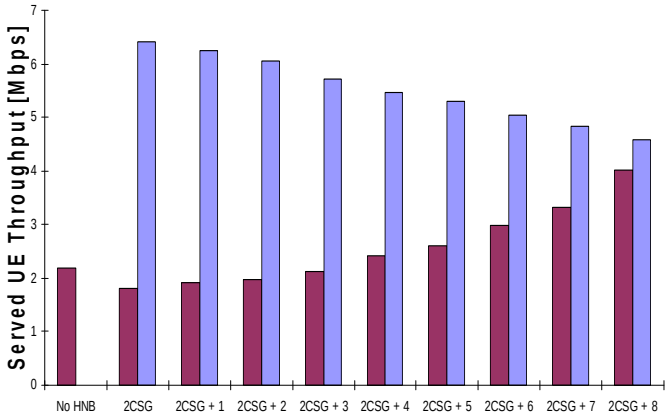

Figure 3.11: HSDPA throughput for UEs in the HSUPA-dominant scenario. The dark/red bars correspond to macro-connected UEs; the light/blue bars correspond to femtocell-connected UEs.

are engaged in HSUPA only, while the remaining 10% are simultaneously using all of HSDPA, HSUPA, and voice. In the two scenarios studied, the UEs engaging in each type of service are chosen randomly in accordance with the probabilities given above. While typical relative usage patterns of different traffic types will obviously vary, exploring these heavily HSUPA- or HSDPA- dominant extremes helps to focus on the specific interaction of traffic type, access policy, and network performance.

Fig. 3.10 considers the HSDPA throughput in the HSDPA dominant scenario. The vertical axis gives the average (per UE) throughput for those UEs connecting to the macro base stations (dark bars), and to the femtocell (light bars). Different positions on the horizontal axis represent different policies for femtocell access. At the left end of the axis, the case with no femtocells is considered. In this case all of the UEs, including the two UEs that will later be part of the CSG, connect (or attempt to connect) to the macro base stations. The next position on the horizontal axis is labeled 2CSG, and considers that performance when the femtocells are present and the access is closed so that only the two CSG mobiles can utilize them. As one moves further to the right on the axis, successively larger

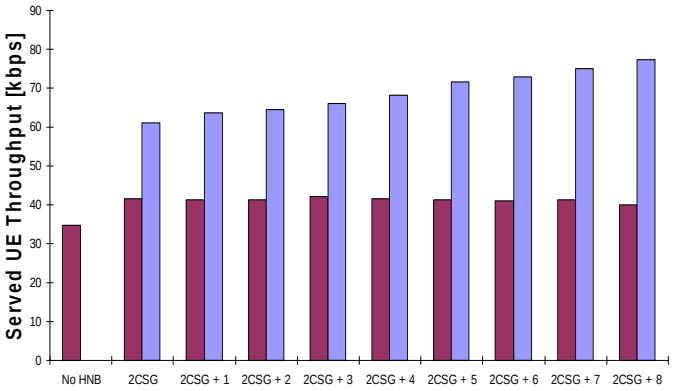

Figure 3.12: HSUPA throughput for UEs in the HSDPA-dominant scenario. The dark/red bars correspond to macro-connected UEs; the light/blue bars correspond to femtocell-connected UEs.

numbers of neighbors are granted access to the femtocells.

As the access policy is changed toward a more open policy, the average femtocell-connected UE throughput decreases. This is because the femtocell needs to share its bandwidth among increasing numbers of neighbors. At the same time, as more users are allowed onto the femtocell, the number of UEs served per each macrocell decreases, so the throughput enjoyed by the macrocell-connected UEs increases.

Fig. 3.11 considers the HSDPA throughput in the HSUPA-dominant scenario. Unsurprisingly, the overall throughput rates are significantly higher than for the HSDPA-dominant case in Fig. 3.10, because in the HSUPA-dominant scenario there are fewer UEs competing for downlink data bandwidth, and downlink interference levels are lower. In addition, the decrease in femtocell-connected UE throughput with increasingly open access is significantly less pronounced than in Fig. 3.10 because, again, there are fewer downlink demands on the femtocell, so the resource sharing that accompanies open access imposes a smaller per-UE penalty.

Fig. 3.12 considers the HSUPA throughput in an HSDPA dominant scenario. Fig. 3.13 considers the HSUPA throughput in an HSUPA dominant scenario. Both

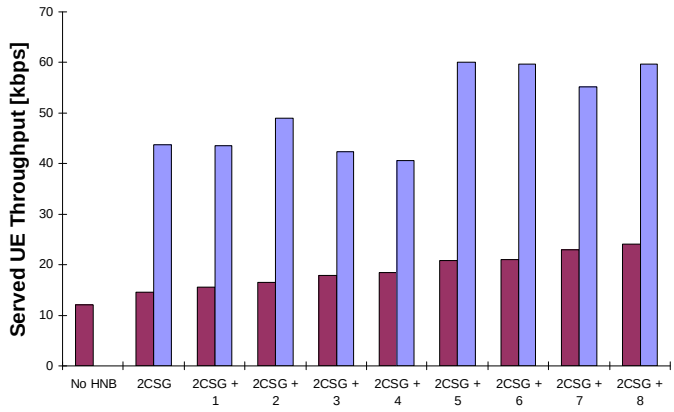

Figure 3.13: HSUPA throughput for UEs in the HSUPA-dominant scenario. The dark/red bars correspond to macro-connected UEs; the light/blue bars correspond to femtocell-connected UEs.

of these figures show that the HSUPA throughput increases with more open access, as contrasted with the decrease observed in HSDPA throughput in Figs. 3.10 and 3.11. This indicates that, for HSUPA throughput, while more open access means that each femtocell shares its resources among a larger group of UEs, with respect to HSUPA, this potential disadvantage is more than outweighed by the increased ability of the femtocell to control the scheduling of UEs in its vicinity. Interestingly, of the four throughput plots in Figs. 3.10 through 3.13, Fig. 3.12 is the only plot in which macro-connected UEs experience a small decrease in average throughput as the femtocell access becomes more open. In fact, each UE that remains connected to the macro base station experiences a relatively small increase in HSUPA throughput with increasingly open access. This small increase is due to a modest decrease in uplink interference levels because with more open access there is a smaller load on the macro base stations (the decrease is modest because the fraction of overall UEs using HSUPA is only 10%). Despite this, the plot shows an overall decrease in macro UE HSUPA throughput because more open access moves increasing numbers of neighboring, high-rate HSUPA UEs onto the femtocell. The loss of these UEs from the pool of macro-connected UEs used

in computing the averages shown in the plot outweighs the improved interference effects noted above. Nevertheless, while the plot is therefore accurate, it does not explicitly convey the fact that from the standpoint of any specific UE using HSUPA in this scenario, the throughput will generally improve with more open access.

3.4 Conclusions

We have examined the impact of femtocell access policy as it relates to network traffic type as well as to the type of base station (femtocell or macro) to which the UEs are connected. It was shown that completely closed access can disrupt service because of the interference generated by UEs that are near to, but prohibited from attempting to connect to, a femtocell. Completely open access can also be problematic due to the loss in data rate arising from sharing limited femtocell bandwidth among potentially large numbers of users. Rather than completely or closing or opening access, better performance can be achieved by opening the femtocell to the best operating point for a given set of goals concerning connectivity and throughput.

In particular, for HSUPA, more open access provides the femtocell with increased opportunities to exert control over the scheduling of HSUPA transmissions for UEs in its vicinity, thus reducing the amount of interference from nearby UEs not connected to the femtocell and leading to higher overall packet success rates. femtocell access policy has a much less significant impact on the PSR of UEs connected to the macro base station, as the UEs connected to the femtocell transmit with much lower power and thus provide less interference.

CHAPTER 4

Scheduling

4.1 Introduction

The present chapter focuses on the scheduling of data packets–specifically in the uplink–in a heterogeneous cellular network consisting of both macrocells and femtocells. The significance of this problem in the case of such networks is the limitations in the connectivity between the femtocells and the provider's network. Such limitations can include high latencies and relatively low data rates, which make operations such as soft hand-offs and fast synchronization impossible to achieve. Hence, what is needed is a scheduling approach that utilizes minimal data overhead and has low latency requirements.

Scheduling in general has been widely studied in topics such as task assignment problems in operations research (see for example [TGS94]), or scheduling of parallel applications in multiprocessor networks [ELA94]. In[CK88] a taxonomy of various scheduling algorithms is presented. In the field of cellular packet data networks several studies have been performed. A fairness criterion introduced by [Kel97] referred to as proportionally fair scheduling is a well known and widely deployed mechanism. In [KW04] it is shown that proportionally fair scheduling converges under various conditions to the solution of a log-sum optimization criterion. In [BLR09], [WOE05], and [SWM08] generalized versions of the proportionally fair optimization criteria are considered.

The uplink scheduling algorithm presented here is based on simulated anneal-

ing, which was first proposed as an optimization method in [KGV83]. Simulated annealing is an iterative optimization technique that has proven to be effective in solving general combinatorial optimization problems. In previous work, simulated annealing has been applied in a wide range of applications including scheduling in parallel systems [LB91], [KGR95], [MS08].

In this chapter, we present a unique application of simulated annealing in the context of uplink packet scheduling in a cellular network. In addition, we introduce an augmented version of simulated annealing that takes specific interference information into account in the optimization process, and present results that support its utility in the developed system framework. We first establish a foundation for the analysis of the optimization and provide necessary conditions on convergence of the proposed algorithm. Our work demonstrates that the use of simulated annealing and augmented simulated annealing with interference awareness for block scheduling improves the QoS experienced by disadvantaged users in a cellular network with minimal signaling overhead.

Our work demonstrates that, in scenarios with Doppler frequencies within the low to normal range, an interference aware scheduling such as the augmented simulated annealing can provide a better QoS experienced by disadvantaged users in a cellular network as compared to a channel aware scheduling, while maintaining minimal signaling overhead. By contrast, in high Doppler frequency scenarios, channel-aware scheduling becomes more effective than interference-aware scheduling. This is because the high mobility ensures that random statistical variations in instantaneous channel quality will create windows of opportunity for higher rate transmission. Exploiting these windows gives more throughput improvement than an approach based purely on interference monitoring.

The rest of the chapter is organized as follows: in Section 4.2 the system framework is defined and the scheduling algorithm is proposed. In Section 4.3 we provide necessary conditions for the convergence of the proposed algorithm.

In Section 4.4 simulation results are presented, and conclusions are presented in Section 4.5.

4.2 System Framework

We consider uplink packet scheduling in a time division multiple access cellular system in which there are N BSs with u_n users registered to each BS $n \in [1, N]$. We define block scheduling as a scheme in which scheduling is performed in predetermined blocks consisting of L time slots. Within each time slot one UE is scheduled. The UEs within the block schedule of a particular BS are not necessarily unique. It is further assumed that these scheduling blocks are repeated in time for the duration of the study.

We assume that a particular UE connects to a BS based on the strongest received pilot signal power. We further assume that all UEs are in fixed positions for the duration of the optimization, and the UE-BS associations are static. The UEs in this multicellular system are characterized based on two traits: 1) their strength of connectivity to their own serving BS (strongly-connected or weakly-connected UEs, referred to as "strong" or "weak" UEs respectively); and 2) the levels of interference generated to neighboring BSs ("interfering" or "non-interfering" relative to a particular BS). The strength of connectivity is based on the link loss experienced between the UE and its associated BS, referred to as the *weakness threshold*. Similarly, the interference characterization is based on the ratio between the interferer's linkloss to its associated BS and its linkloss to another BS, referred to as the *interference threshold*. A "collision" occurs when a weakly connected UE is scheduled concurrently with an interfering UE from a neighboring cell. Therefore, the block schedule of a particular BS is compared to those of all the remaining $N - 1$ BSs on a per time slot basis to determine the occurrence of collisions.

We consider three scheduling schemes: round robin (RR) scheduling, block scheduling with simulated annealing (BS-SA), and block scheduling with augmented simulated annealing (BS-ASA). We proceed by first describing the simulated annealing algorithm, and then describing the BS-SA and BS-ASA algorithms as its derivatives in the context of uplink packet scheduling.

```
INITIALIZE
repeat
  PERTURB(state i → state j, ΔC_ij)
  if ΔC_ij <= 0 then
    ACCEPT
  else
    if exp(−ΔC_ij/T) > random[0, 1] then
      ACCEPT
    else
      REJECT
    end if
  end if
until equilibrium is approached sufficiently closely.
```

Figure 4.1: Pseudo-code describing the simulated annealing algorithm.

4.2.1 Simulated Annealing

Simulated annealing is a generic iterative optimization method where random mutations in a state variable occur at each iteration. The algorithm is summarized in the pseudo-code given in Fig. 4.1 [LA87].

At the end of the iteration, the simulated annealing algorithm compares the mutated state to the current state and probabilistically decides whether to transition to this state or remain in the previous state. If the cost of the mutated state

is lower than that of the current state, then a transition to the mutated state occurs. Otherwise, the mutation is accepted with a probability given by $e^{-\frac{\Delta C}{T}}$ (referred to as the acceptance probability [LA87]), where ΔC is the difference in cost between the mutated state and the previous state and T is the temperature, which is used as a control parameter. The mechanism of accepting cost-increasing mutations is implemented to avoid convergence to a local minimum.

4.2.2 Block Scheduling with Simulated Annealing (BS-SA)

Applying the simulated annealing algorithm to block scheduling, we derive the BS-SA scheme. The system state we consider in BS-SA is the combined block schedule for all N BSs in the system. It is assumed that every BS uses block scheduling with the same block size of L, where $L \gg \max(u_1, ..., u_N)$, and the block schedules on the BSs are synchronized. The cost function considered is the total number of collisions per block.

The mutated state is one in which two time slots in the block schedule for *every* BS are randomly switched. A central entity (such as the radio network controller) receives information on the number of collisions each BS experiences after every block and assesses the difference in the collision rates between the mutated state and the current state. It will then compute the acceptance probability for the mutated state and send a message to each BS to determine whether the BS should accept the mutation or not.

Note that under this scheme the overhead signaling imposed on the BS for each scheduling block is minimal and includes only a collision measurement transmitted to the network and an accept/reject signal received back. Possible latencies in the arrival of the accept/reject notifications from the central network come at an insignificant cost: the BS can simply continue its current schedule into the next block for a few time slots until the arrival of the notification. The expected number

of differences between the old and the new schedules in these time slots is small.

It is worthy of mention that one could also consider the application of simulated annealing in which only one switch in the entire system state is applied at each iteration. Such a scheme would significantly reduce the optimization speed and is prohibitively slow, and hence is not considered by the authors.

4.2.3 Block Scheduling with Augmented Simulated Annealing (BS-ASA)

While the collision information is utilized at the decision making stage of the BS-SA, this data is disregarded at the mutation stage where switches are performed between any two randomly chosen slots. Block scheduling with augmented simulated annealing (BS-ASA) is a modified version of the BS-SA in which the collision information is used in choosing the time slots that will be switched. Explicitly, the mutated state considered is a random switch between every time slot in the block schedule in which a single collision occurs with another randomly chosen time slot in the block. A faster convergence rate for this algorithm is expected and is observed in the simulation results presented in Section 4.4.

4.3 Convergence Analysis

In this section we establish an analytical framework related to the convergence of both the BS-SA and BS-ASA algorithms. Our attention will be focused on the homogeneous algorithm in which the temperature, T, is kept constant. The optimization process is modeled as a Markov chain where we define the state of the system to be the collection of all the individual block schedules (as mentioned previously in Section 4.2):

$$i^k = \bigcup_{n=1}^{N} i_n^k, \tag{4.1}$$

where $i_n^k = \left[M_{n,1}^k, M_{n,2}^k, \cdots, M_{n,L}^k\right]$, N is the number of BSs, i_n^k is BS n's block schedule at the kth iteration, and the UE scheduled at index l of BS n's block schedule at the kth iteration is denoted as $M_{n,l}^k$, and $l \in [1, L]$. It is noted here that the state space R is not the set of all permutations of the UEs in the state vector, but only the subset of those permutations in which the UE-BS associations have been kept the same. The resulting total state space size is then $(L!)^N$. The transition probability matrix of the optimization process as described in [LA87] is:

$$P_{ij}(k) = \begin{cases} G_{ij} A_{ij}(k), & i \neq j, \\ 1 - \sum_{l \neq i} G_{il} A_{il}(k), & i = j, \end{cases} \tag{4.2}$$

where G_{ij} is the probability of state j being generated from state i, and $A_{ij}(k)$ is the probability of the generated state j being accepted from state i. In the conventional simulated annealing algorithm, where all mutations are equally likely, G_{ij} is given by:

$$G_{i,j} = \begin{cases} 0, & for\ j \notin R_i, \\ \frac{1}{|R_i|}, & for\ j \in R_i, \end{cases} \tag{4.3}$$

where R_i is the set of all states accessible from state i in one random mutation (the neighbor set). The admittance probability matrix as a function of the temperature is given by:

$$A_{ij}(k) = \begin{cases} 1, & C(j) < C(i), \\ e^{-\frac{C(j)-C(i)}{T(k)}}, & C(j) > C(i). \end{cases} \tag{4.4}$$

Convergence of this process to steady state will be conditioned on irreducibility and aperiodicity of the underlying Markov chain. This is explored in the following subsections.

4.3.1 Aperiodicity

To establish aperiodicity in a Markov chain it is sufficient and convenient to simply prove that there is a non-zero probability of staying in a state, i.e. $\exists i : P_{i \to i} > 0$.

Formally we can prove the existence of such a state as follows.

Proof. Let the process begin in a globally optimal state, $i^1_{opt} \in R_{opt}$, where R_{opt} is the set of all globally optimal states. After a single iteration of switches on an optimal state, a new state is generated. Such a state can be generated according to two cases. In the first case, a non-optimal state i^2 that is cost-increasing is considered. Then the original state i^1_{opt} proves aperiodicity due to a non-zero probability of rejected admission for $P_{i^1_o \to i^2} = e^{-\frac{\Delta C}{T}} < 1$ where $\Delta C = C\left(i^2\right) - C\left(i^1_o\right) > 0$ and $T > 0$.

In the second case, the second state can be another optimal state $i^2_{opt} \in R_{opt}$. Then, assuming irreducibility and $R_{opt} \neq R$, after enough iterations we will arrive at a non-optimal state i^k, in which case the optimal state i^k_{opt} proves aperiodicity. □

4.3.2 Irreducibility

We now focus on conditions under which irreducibility can be achieved. Irreducibility of a Markov chain is guaranteed if $\forall i, j \in R$, $\exists k \in : P^k_{i,j} > 0$, i.e. there is a possible path between any two states in the chain. Obviously at $T = 0$ this condition is not met since no cost-increasing mutations are admitted therefore we study only the cases in which $T > 0$. The analysis is performed separately for the conventional simulated annealing and the augmented version presented in this chapter.

4.3.2.1 Irreducibility for BS-SA

In the case of conventional simulated annealing, if we allow only one BS to mutate at each iteration then irreducibility is guaranteed: there will always be a set of mutations that connect any two arbitrary states. Such an algorithm is very slow

in convergence, hence we consider the cases where each BS performs a mutation at each step. If a mutation is forced at each BS, irreducibility is not guaranteed. For a counter example consider the set of two BSs, BS1 and BS2, i.e. $N = 2$, each of which is connected to an independent set of three UEs indexed 1, 2, and 3, $u_1 = u_2 = 3$. Let the state vector be $[\bar{v_1}; \bar{v_2}]$, where $\bar{v_1}$ and $\bar{v_2}$ represent the block schedule for BS1 and BS2, respectively. Fig. 4.2 represents the state transition graph for a BS with a block schedule for $L = 3$. Suppose we start from an initial state of [3,2,1; 3,2,1], and target an end state of [1,2,3; 1,3,2]. Here BS1 will need an odd number of transitions to arrive at its target, while BS2 will need an even number of such transitions and hence the target state will never be achieved simultaneously for both BSs. In order to overcome this obstacle we will need to allow for idle transitions at BSs, in which case each BS can perform the number of required mutations to arrive at the target and stay idle afterwards while others arrive at their target states.

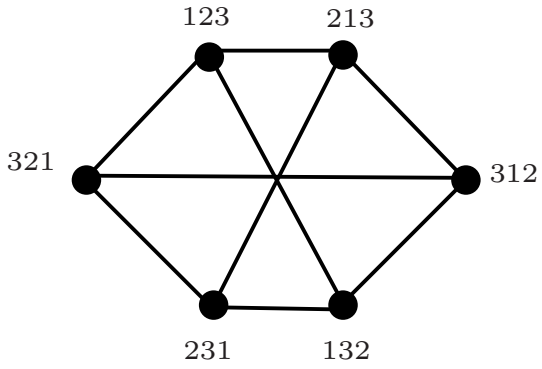

Figure 4.2: State diagram for a BS with 3 associated UEs.

4.3.2.2 Irreducibility for BS-ASA

The BS-SA algorithm will not provide for irreducibility in general. For example, consider a BS that has no interfering UEs connected to its neighboring BSs. In such a case no mutations will be performed on this BS schedule, since no collisions

are detected. With respect to performance, this will be acceptable only if the UEs connected to this BS are not interferers to their neighbors. Where interferers exist, however, the schedule of the interferers is of concern to the network and needs to be flexible.

We consider two cases in which such irreducibility is guaranteed. The first case considers combining BS-SA and BS-ASA and allowing for random mutations performed independently of the collisions. Here, again, all mutations are possible and therefore there exists a path between any two states.

The second case is a model in which the interference is not perfectly known, and is only detected by the BS that receives the uplink data. Furthermore, detection of such interference is performed by the BS on all upcoming data, regardless of whether the UE from which the data is being received is weak or strong. In this case, once again, any UE can be detected as being under interference from the neighborhood, and can possibly be mutated in its schedule.

While in both cases mentioned above, irreducibility comes at the cost of slower convergence, in the second case the lack of perfect knowledge incurs the extra cost of instability at the global optimum: any false detections can bring the system out of the global optimum after it is reached.

4.4 Simulation

In this section we present the collision rates for the algorithms presented in Section 4.2. A scenario featuring 14 BSs and 200 UEs is studied on a 4000 meter by 4000 meter 2D map. Constant, full buffer uplink traffic is considered for each UE. An ideal channel is assumed and a simplified path loss model is used. A block length of $L = 200$ time slots is used and a weak distance threshold of 600m is set along with an interference threshold of 1.3. Note that under a static scenario distance translates to a constant link loss. Simulation results are shown in Fig. 4.3

as collision rates per slot. A temperature of $T = 0$ is used with both BS-SA and BS-ASA. With RR showing the expected constant collision rate, we observe sluggish improvement in the collision rates under the BS-SA algorithm as compared to the BS-ASA. For both the BS-SA and BS-ASA algorithms a temperature of zero means that there is no guaranteed irreducibility, however the convergence to a zero collision rate is still possible. What is further observed is that disregarding the collision information when making the random switches in the block schedule is shown to be extremely costly to the performance of the optimization, to the point that it renders the BS-SA method impractical for implementation for cellular environments because of its extremely slow rate of convergence as observed in Fig. 4.3.

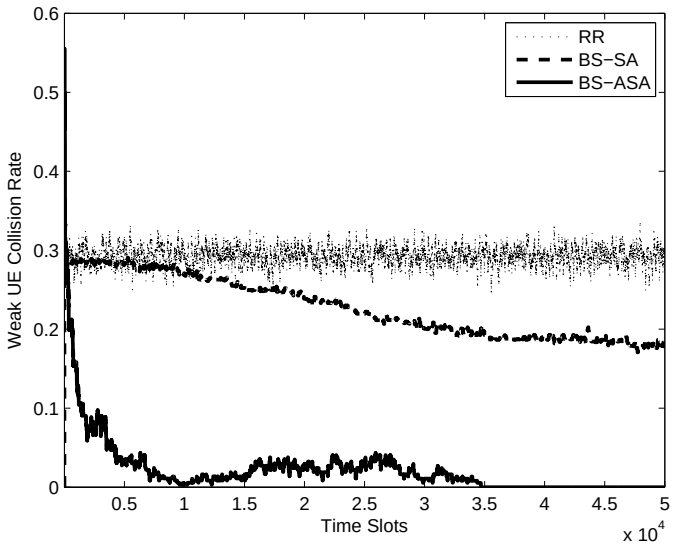

Figure 4.3: Weak UE collision rates for RR, BS-SA, and BS-ASA algorithms.

From the perspective of a network operator, an optimization algorithm must be fast enough to cope with the variations in the scenarios, such as hand offs and deep fades. Considering that such events occur in the order of magnitude of once every few seconds, the optimization must be likely to convergence to almost-optimal solutions in similar lengths of time with high probability. In our study, the BS-

ASA optimization was reiterated numerous times for the same scenario described above. After 1000 independent runs the cumulative distribution function (CDF) for convergence to various collision rates was extracted as a function of the number of time slots and plotted in Fig. 4.4. The BS-ASA is shown capable of achieving a 10% collision rate with 90% probability after 4000 time slots, which proves to be a feasible performance criterion for cellular networks. Fig. 4.4 also illustrates the CDF for collision rates of achieving less than 5% and 0% collision rates serving as additional performance criteria.

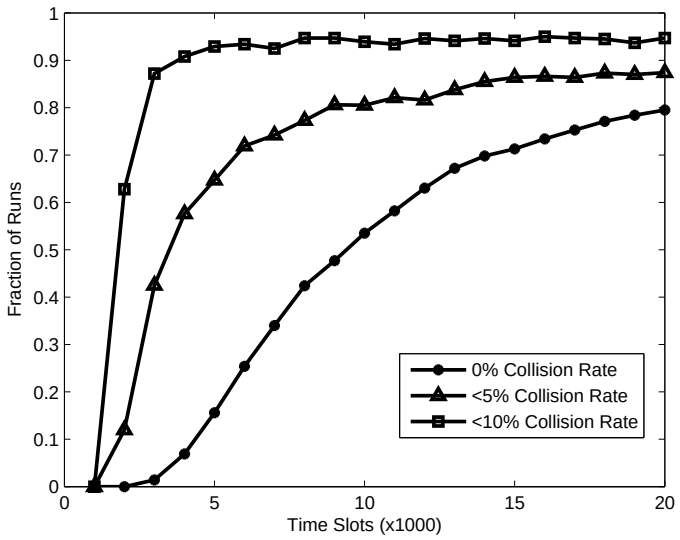

Figure 4.4: CDFs for convergence of BS-ASA for three different target collision rates.

In order to assess the performance of the BS-ASA under imperfect collision detection, the same simulation was performed using multiple pairs of false alarm and misdetection probabilities for weak UE's, noted as P_{fa} and P_{md} respectively. Results, as shown in Fig. 4.5, show that the algorithm is far more vulnerable to false alarm rates than to misdetection rates, hence the collision detection scheme must be designed biased towards misdetections. This bias is due to the fact that the number of collisions is a small fraction of the total number of packets

scheduled, and hence a small fraction of false alarms on the non-collision slots can have the same effect as a large fraction of misdetections on the collision slots.

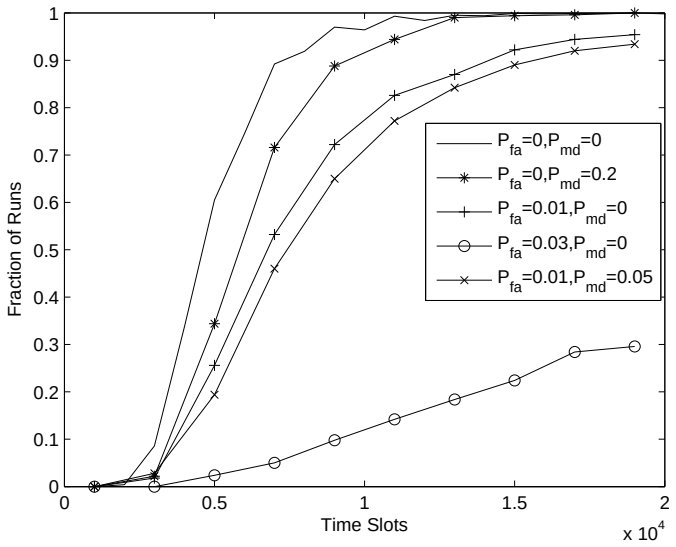

Figure 4.5: CDFs for convergence of BS-ASA to 10% collision rate for various weak UE false alarm and misdetection probabilities.

In order to compare the performance between BS-ASA and PF scheduling schemes, it is notable that the proportionally fair algorithm as defined in [KW04] assumes perfect knowledge of both the channel state and the interference level at the time of transmission. While the former can be attained with a reasonable level of accuracy, the interference levels are difficult to predict in a network with highly dynamic behavior and low inter-BS coordination. Therefore we implement a channel-aware version of the PF algorithm to be compared against BS-ASA. Shown in Fig. 4.6 are plots comparing the performance of the two schemes under four different Doppler conditions. We observe that under the small Doppler frequencies where channel variation levels are low, the interference aware BS-ASA scheduling shows superior results, while in the highest Doppler frequency the channel variations become more important to take advantage of, giving the superiority to the PF scheduling.

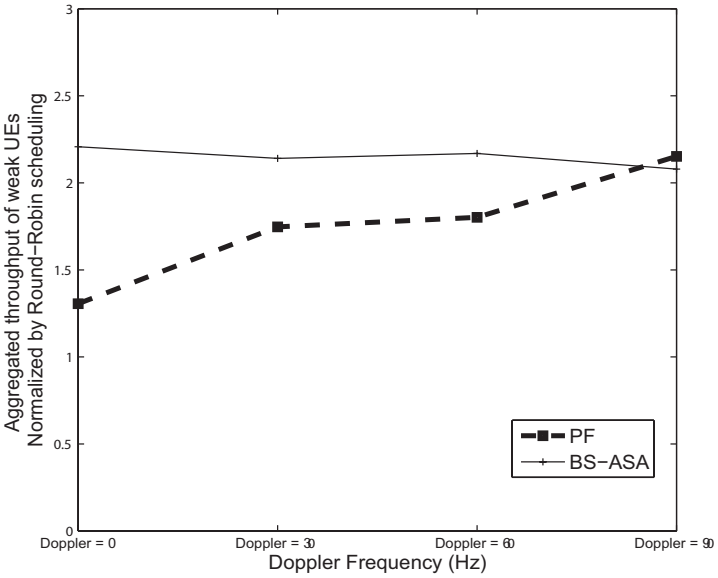

Figure 4.6: BS-ASA and PF throughput gains relative to RR for weak UE's for different Doppler scenarios.

4.5 Conclusion

In this chapter we propose the use of an augmented version of simulated annealing for scheduling in heterogeneous networks. An analytical framework is provided for the modeling of such algorithms, along with the analysis of necessary conditions for convergence of the algorithms to optimum. Simulation results are provided to demonstrate the advantages of the BS-ASA to the conventional BS-SA, and establish feasibility for implementation of such algorithms in femtocell networks. Furthermore, results are provided showing the trade-off between channel awareness and interference awareness in scheduling under different mobility conditions.

CHAPTER 5

HandOff Management

5.1 Introduction

This chapter addresses the issue of hand off management, which has been classically approached in multiple different ways. The state of the art approaches have mostly focused on issues such as continuity of service, load balancing between base stations, and providing minimum QoS requirements. Here we aim to address a specific issue that arises in the context of femtocell deployments, which is the possibility of large and unnecessary overhead in a network where femtocells are densely deployed. We propose a predictive algorithm with the aim of minimizing the number of hand offs in such scenarios. This performance measure is used to compare the proposed algorithm against a primitive method for managing the hand-offs in mobile networks, namely connecting at any time to the base station perceived with higher power by the mobile station.

Work in predictive algorithms for mobile networks is not extensive. In many of the studies prediction is used as a means to pre-allocate resources on base stations prior to the arrival of a mobile station into the cell [**?**], [**?**], [**?**]. In the proposed approach the predictive algorithm is executed in the mobile station, assuming necessary information has been communicated between the network and the mobile station that allows for computation to be performed. Additionally, the mobile station's positioning ability can facilitate the prediction of the user trajectory. Our technique is aided by real world data about road topology, road-

traffic statistics and vehicle speeds.

An important measure of call quality is minimal call drop probability. Incorporated in the model is a minimum receive power requirement, which is added as additional constraints to the algorithm to ensure that any subsequent handoffs will be providing the minimum QoS requirement with a high probability.

The theoretical framework of our algorithm is based on Markov model. This model is applied to a statistical traffic model incorporating road information in a scenario. The prediction framework is explained in Section 5.2. This is followed by simulation results provided in Section 5.3 followed by conclusions in Section 5.4.

5.2 System Framework

Presented in this section is the framework for the predictive handoff minimization algorithm. The objective is minimizing the number of hand-offs while maintaining the QoS requirement.

Assumed in the model is the knowledge of road topography in the scenario, as well as road traffic speeds and transition probabilities at intersections (ie. turn likelihoods).

In Fig. 5.1 a simple scenario is shown where the path followed by the mobile station is known and indicated by the arrow. A, B, C and D are the areas under the coverage of certain base stations where the QoS is satisfied. In the overlapping areas, the QoS is satisfied by more than one base station. We define a tile as an area on the map where an exclusive set of base stations can meet the QoS requirement.

First the path is divided into N segments, each of them associated with one tile. In Fig. 5.1 we have 6 segments along the mobile station path. With the conventional hand-off technique of choosing the most powerful signal, the base

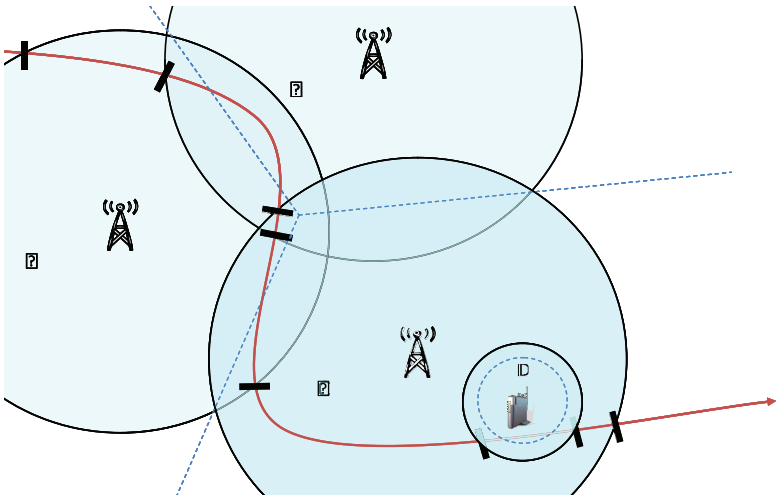

Figure 5.1: Sample mobile station path through a multi-base station scenario

station sequence would be as follows: A-B-A-C-D-C, while the optimal assignment for minimizing the number of base station changes would be A-A-A-C-C-C. In the following passages, first a continuous model is presented in Section 5.2.1, followed by a discretized version of the algorithm in Section 5.2.2. An additional constraint added for ensuring QoS is discussed in Section 5.2.3.

5.2.1 Mathematical formulation, Continuous case

We can model the motion of the mobile station as a continuous-time Markov process. Hence, the probability density of the future paths is predicted given its recent history of locations and speeds as:

$$f(x(\tau, t < \tau < t + T)) = f(x(\tau, t < \tau < t + T)|x(\tau', t - T_p < \tau' < t))$$

We define the objective as to find the base station k^* that minimizes the expected number of handoffs looking forward:

$$k^* = \arg\min_{k \in B} \{ \underset{p \in \phi}{E} [\Theta(r_{opt}(p|r_1 = k))] \}$$

In the above equation B is the set of all base stations, p represents one path, ϕ is the set of all predicted paths for the future T_f seconds, Θ indicates the number of hand-offs in a given sequence of base station assignments r, and $r_opt(p|r_1 = k)$ is the optimal sequence of base station assignments conditioned on the first base station being k:

$$r_{opt}(p|r_1 = k) = \underset{r \in R_p | r_1 = k}{\arg\min} \{\Theta(r_1 = k, r_2, \ldots, r_{N_p})\}$$

Where R_p represents the set of permissible base station assignments for path p:

$$R_p = \{r | r_n \in \Gamma_{p_n}, \forall n : 1 \leq n \leq N_p\}$$

N_p represents the number of segments in path p, and Γ_{p_n} is the set of base stations meeting the QoS target for the n^th segment of path p.

In the following section a discretized version of the above formulation is presented.

5.2.2 Discrete Approach

Under the discrete formulation a state graph is generated demonstrating the possible tiles in which a mobile station can be located in discrete times looking forward.

Shown in Fig. 5.2 is the state graph generated using the Markov model, with each node representing the presence of the mobile station in a tile, and each arrow representing a tile crossing event (or lack of it) in ΔT seconds with a known probability. For all states there is a non-zero probability of staying in the same tile (no transition). The depth of the graph or number of stages in each branch theoretically determines the tradeoff between better accuracy of prediction and computational complexity.

The model is now as follows:

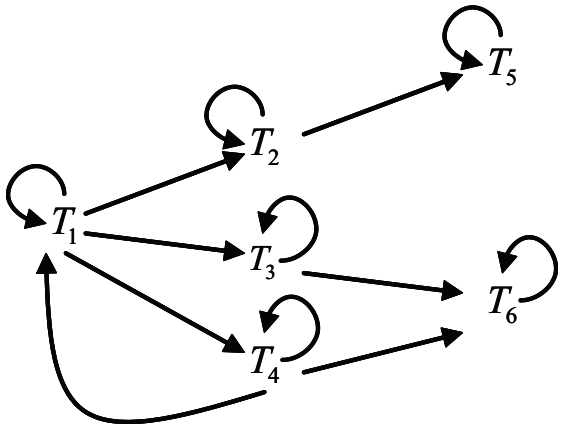

Figure 5.2: Tile graph based on Markov model (discrete time)

$$k^* = \underset{k \in B}{argmax} \{ \underset{p \in \phi}{E} [I(r_1^{opt}(p) = k)] \}$$

Where B is the set of all base stations, p represents one path along the graph, Φ is the set of all predicted paths over the graph with a length of $T_f/\Delta T$, I is the indicator function, and $r_1^{opt}(p)$ is the first base station in the optimal sequence of base station assignments for path p:

$$r_{opt}(p) = \underset{r \in R_p}{\arg\min} \{\Theta(r_1, r_2, \ldots, r_{N_p})\}$$

Where R_p represents the set of permissible base station assignments for path p :

$$R_p = \{r | r_n \in \Gamma_{p_n}, \forall n : 1 \leq n \leq N_p\}$$

N_p represents the number of nodes in path p, and Γ_{p_n} is the set of base stations meeting the QoS target for the n^{th} node of path p.

5.2.3 Presence Constraint

We introduce an additional constraint to ensure the support of QoS requirement after the mobile station is handed over to a new base station. Referred to hereafter as the presence constraint, it measures the probability of a base station being

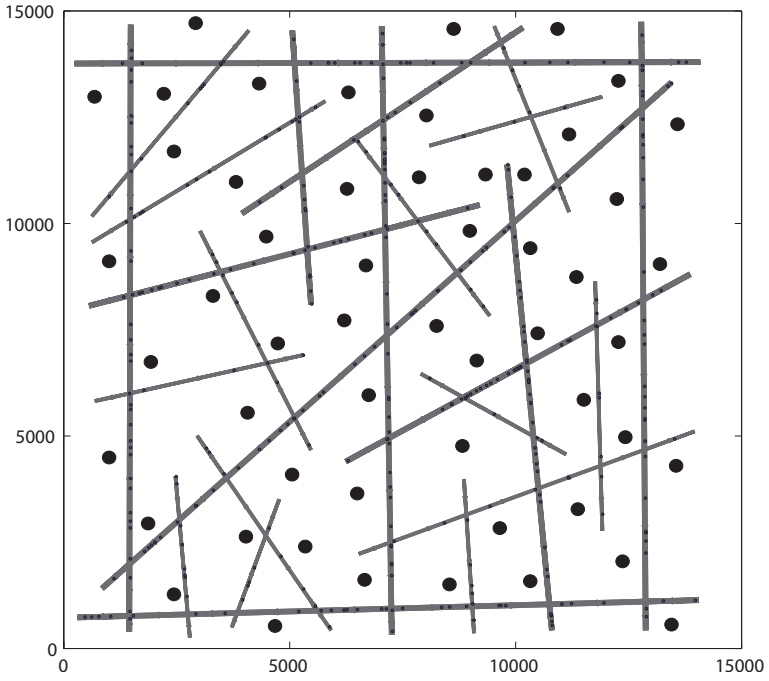

Figure 5.3: Macrocell only Scenario

supported in the next step of the prediction. A threshold is used on this measure to ensure the likely support of the QoS after transition. This constraint is formulated as follows:

Where P_{QoS} is the probability of meeting the QoS target in terms of presence,I represents the indicator function, Γ is the set of base stations that meet the QoS target in a given path segment, and p_1 is the first segment of the path p.

5.3 Results

The predictive hand off algorithm was simulated in a series of scenarios. One such scenario has been displayed in Fig. 5.3, wherein the black dots represent base stations and the blue ones mobile stations. The scenario contains 400 mobile stations and 45 base stations, distributed almost uniformly throughout.

During the simulations multiple parameters have been varied to observe the

behavior of the system under different configurations. The parameters include the coverage radius, the prediction depth, and the density of Femto base stations deployed (0 in Fig. 5.3). Each simulation has been run over 600000 time slots representing 10 minutes of real time traffic. The simulations use the Okumura-Hata link loss model.

5.3.1 Varying the Coverage Radius

There are trade-offs involved in minimizing the number of hand-offs in the cellular network. One drawback is that when a mobile station is connected to a base station other than the one with smallest link loss, it will likely experience smaller data rates (assuming similar loading on the base stations). The solution lies in tuning the minimum coverage radius for the base stations - or equivalently, the minimum received power. We have simulated four different coverage radii using both the predictive algorithm and instantaneous largest pilot strength. Results are presented in Fig. 5.4.

As the coverage radius is raised, the number of hand-offs decrease since the mobile station is allowed to stay for a longer time under the coverage of the same base station, decreasing the number of hand-offs. The number of handoffs under the predictive algorithm is also lower than the instantaneous pilot case for every radius.

Additionally, the throughput is observed to decrease using the predictive algorithm, diminishing further as the coverage radius is increased. This trend is due to the fact that if the coverage radius is bigger, we are allowing communications over longer distances with less power, lowering the QoS threshold.

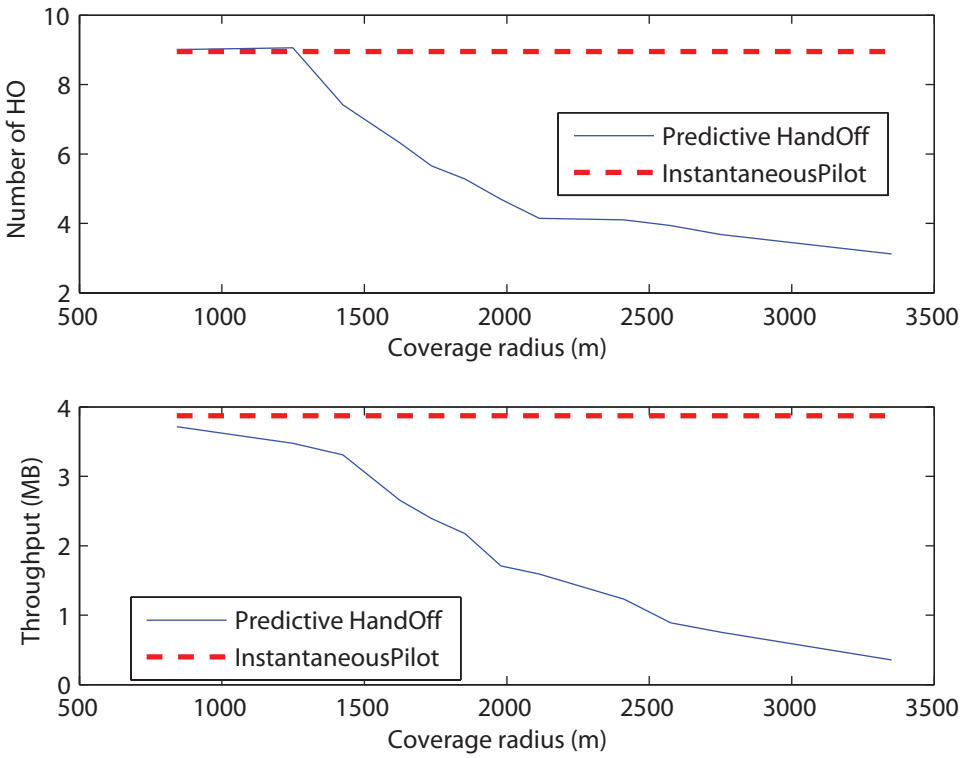

Figure 5.4: Average number of hand-offs and throughput as a function of coverage radius. (predictive algorithm depth 2)

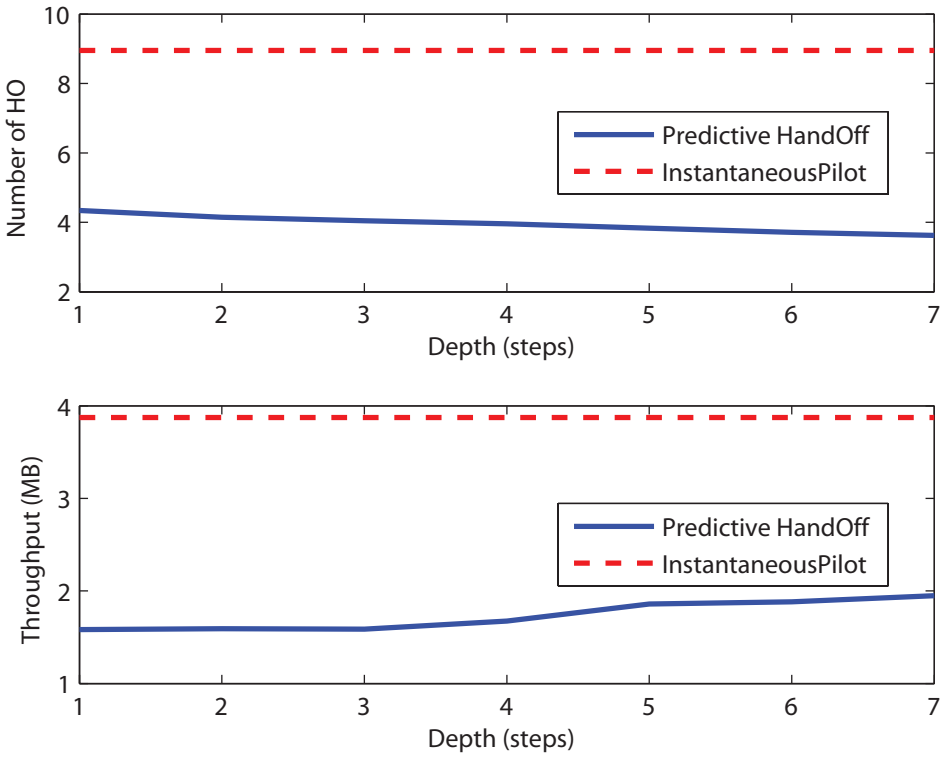

Figure 5.5: Average number of hand-offs and throughput as a function of algorithm depth. (coverage radius 2.1 km)

5.3.2 Varying the Depth

We can simulate for different depths of the predictive algorithm. The average number of handoffs and the throughput are shown in Fig. 5.5 as a function of the depth. The number of handoffs is reduced as the depth of the algorithm is increased, due to the better accuracy in the prediction. On the other hand, the throughput increases with the depth, which means that increasing the depth we obtain better results: fewer handoffs and more throughput.

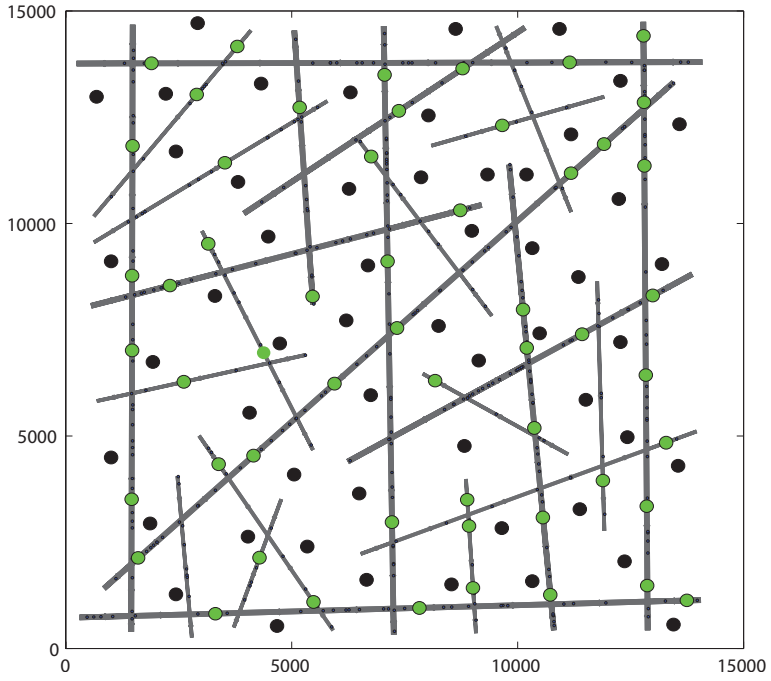

Figure 5.6: Scenario with 54 additional Femto base stations

5.3.3 Including the Femto Base Stations

In this stage we include femto base stations in our simulation, modeled as base stations working at smaller power and, as a result, with a lower coverage radius. We have distributed the femto base stations uniformly in the same scenario, and have simulated using different densities of base stations. For example, in Fig. 5.6 the scenario with 54 femto base stations is shown.

Using the simulations we aim to prove that the predictive algorithm keeps the mobile stations attached to the Macro base stations, avoiding unnecessary handoffs to short-term femtocells. It is known that under a maximum instantaneous pilot scheme the mobile station is going to switch to a femtocell as soon as its power is the highest reachable. With the small coverage radius of the Femto base stations however it is a waste of energy, signaling, and time slots to switch to them just for a short period when the mobile station is able to be served by a nearby macro base station for the entire time. The average number of handoffs

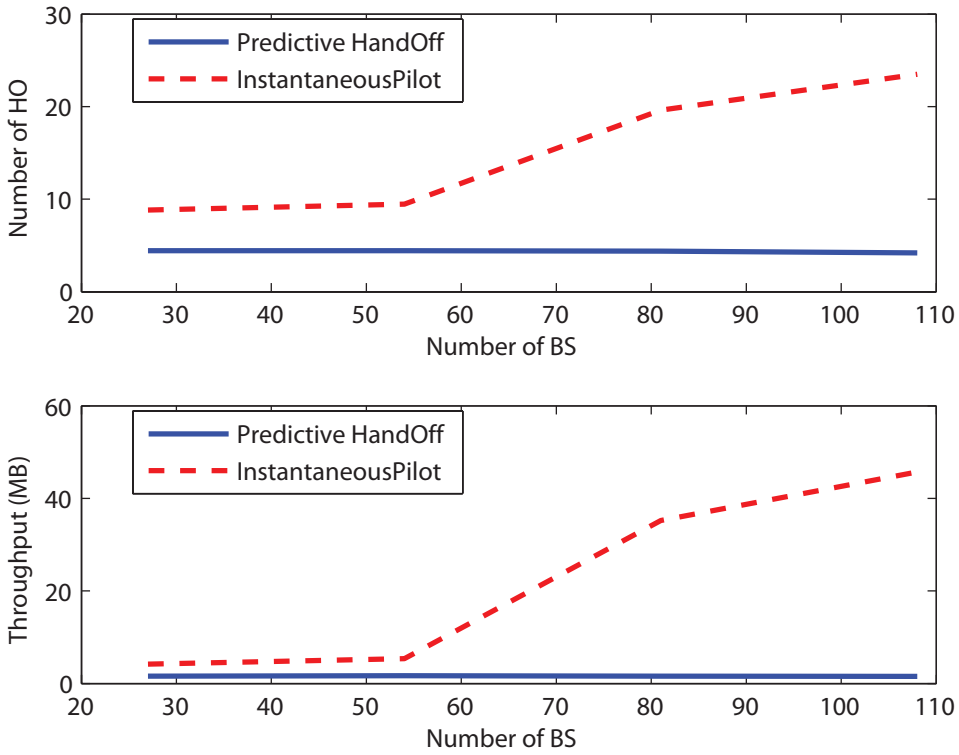

Figure 5.7: Average number of hand-offs and throughput as a function of the number of Femto base stations. (coverage radius 2.1 km)

and the throughput are shown in Fig. 5.7. The results for the predictive case are consistent, showing that the deployment of the femto base stations has introduced no further handoffs and users have been continually served by the macro base stations. That is while the number of handoffs and the throughput increase for the instantaneous pilot scheme.

5.4 Conclusion

Presented in this chapter was a predictive algorithm for minimizing the number of hand-offs in mobile wireless networks. Noting that the aim is to avoid unnecessary handoffs to a small-radius femtocell we have presented results that have

confirmed the functionality of the algorithm in such scenarios by using traffic and motion information. The average number of handoffs in femtocell deployments was shown to be almost equivalent to those of macrocell-only scenarios, which can be a positive aspect in ensuring continuous coverage with minimal handoff disruption for moving mobile station. The tradeoff in such a decision is the instantaneously achievable data rates, which enjoy larger values when the mobile station is connected to a close-by femtocell. The trade-off curves have been derived from simulations, however it is notable that signaling overhead for handoffs have been omitted from the results. In a real-world scenario the users are expected to suffer from intermitted connections, which can be highly undesirable for certain services, most notably voice. Many improvements are possible in this model including higher-order Markov models of the traffic, inclusion of service type in decision making, and integration of access mechanisms discussed in previous chapters.

CHAPTER 6

Conclusions

Developments in simulation for 3G and 4G cellular networks, studies on femtocell access policy, and a novel simulated annealing-based scheduling scheme were presented in this work.

Two system-level simulators for 3G and 4G systems were described in Ch. 2. These tools were built with a few goals in mind that include agility, ease of use and analysis, and speed. Particular attention was paid to flexibility in choosing between various schemes in each aspect of the simulation and removing any dependencies on a specific mechanism that cannot be replaced in future. The simulation tools were the main platform through which all of the algorithms discussed in forthcoming chapters were implemented, tested, and analyzed.

In Ch. 3 access policies to femtocell were studied and it was argued that in a network of both femtocells and macro base stations a limited access policy can provide benefits relative to a completely closed or completely open access policy. The problem, posed solely from the viewpoint of network performance, was explored in a spectrum of possible implementation strategies. For example, and in particular, it was noted that the Closed Subscriber Group can in fact benefit from opening limited access to nearby users, who otherwise can detrimentally impact the instantaneous link quality of the CSG users.

One must note however that the overall problem involves business cases and economic incentives that cannot be fully expanded in this work. It is however hoped that any implementation decisions will be based on informed and educated

sources that include network impacts.

The BS-ASA scheduling scheme was proposed in Ch. 4 as a candidate for implementation in heterogeneous networks in which quick synchronization between base stations is not feasible. An analytical framework was provided for the modeling of such algorithms, along with the analysis of necessary conditions for convergence of the algorithms to optimum. The simulation tools described in Ch. 2 were used to produce results that demonstrate the feasibility of this scheme, along with comparisons to a localized approach. The convergence time of the system was shown to be sufficiently small in normal deployments. Furthermore, results are provided showing the tradeoff between channel-based and interference-based approaches in scheduling under different mobility conditions. From the perspective of weakly connected mobile stations, it was observed that an interference-based approach can be beneficial compared to a channel-based one at lower Doppler frequencies while a channel-based approach can gain the higher edge at higher Doppler frequencies by introducing deeper fades that can be taken advantage of in a channel-aware scheduling scheme.

Presented in Ch. 5 was a predictive algorithm for minimizing the number of hand-offs in mobile wireless networks. The predictive algorithms, implemented in its discrete time variant has been shown to be capable of avoiding unnecessary handoffs to small-area femtocells thereby reducing the amount of signaling and possible disruptions in service. The tradeoff against throughput has been demonstrated, showing that choosing a maximum instantaneous pilot power for handoff decisions could provide greater instantaneous data rates. The final decision making on the level of hand offs however includes factors such as service types, access policy, and signaling overhead that has not been accounted for in the throughput study.

There are many paths for further studies in the field of resource allocation for heterogeneous networks. Service types and queue lengths can be taken into

account in scheduling, access, and handoff schemes. In scheduling, a mixture of channel-aware and interference-aware approaches can be proposed based on the weak-strong-interfering UE distributions. Such a scheme can use Bayesian approaches when deciding between the approaches. Furthermore users categorizations can be improved by taking into account service types as well as link quality. Finally, in handoff decisions, the sensitivity of the service to delay and disruption and its data rate requirements can be taken into account when making a predictive handoff decision.

It is hoped that this body of work as well as future advances can impact the quality of femtocell deployments, generating a strong business and scientific case for greater attention to these capable and agile devices.

References

[BBR99] A. Bedekar, S.C. Borst, K. Ramanan, P.A. Whiting, and E.M. Yeh. "Downlink Scheduling in CDMA Data Networks." In *Proc. of IEEE Global Telecommunications Conference*, volume 5, pp. 2653–2657, December 1999.

[BLR09] Tian Bu, Li Li, and Ramachandran Ramjee. "Generalized Proportional Fair Scheduling in Third Generation Wireless Data Networks." In *IEEE Proc. of INFOCOM, Barcelona, Spain*, pp. 1–12, April 2009.

[CK88] Thomas L. Casavant and Jon G. Kuhl. "A Taxonomy of Scheduling in General-Purpose Distributed Computing Systems." *Euro. Trans. Telecommun.*, **14**(2):141–154, February 1988.

[ELA94] Hesham El-Rewini, Theodore G. Lewis, and Hesham H. Ali. *Task Scheduling in Parallel and Distributed Systems.* Prentice Hall, Englewood Cliffs, New Jersey, 1994.

[Kel97] Frank Kelly. "Charging and Rate Control for Elastic Traffic." *Euro. Trans. Telecommun.*, **8**:33–37, May/June 1997.

[KGR95] K. Krishna, K. Ganeshan, and D.J. Ram. "Distributed simulated annealing algorithms for job shop scheduling." *IEEE Trans. Syst., Man, Cybern.,*, **25**(7):1102 –1109, July 1995.

[KGV83] S. Kirkpatrick, C.D. Gelatt, and M.P. Vecchi. "Optimization by Simulated Annealing." *Science*, **220**(4498):671–680, May 1983.

[KW04] Harold J. Kushner and Philip A. Whiting. "Convergence of Proportional-Fair Algorithms under General Conditions." *IEEE Trans. on Wireless Commun.*, **3**(4):1250–1259, July 2004.

[LA87] P.J.M. van Laarhoven and E.H.L. Aarts. *Simulated Annealing: Theory and Applications.* D. Reidel Publishing Company, Dordrecht, Holland, 1987.

[LB91] Z.-P. Lo and B. Bavarian. "Job scheduling on parallel machines using simulated annealing." In *IEEE Trans. Syst., Man, Cybern., 1991. 'Decision Aiding for Complex Systems, Conference Proceedings.*, pp. 391 –396 vol.1, October 1991.

[LW01] J. Laiho and A. Wacker. "Radio Network Planning Process and Methods for WCDMA." *Annals of Telecommunications*, **56**(5-6):317–331, May 2001.

[MS08] R.F. de Mello and L.J. Senger. "On Simulated Annealing for the Scheduling of Parallel Applications." In *20th Int. Symp. on Comp. Arch. and High Perf. Comput., 2008. SBAC-PAD '08.*, pp. 29 –36, November 2008.

[Nok07] Nokia Siemens Networks. "Initial Home NodeB Coexistence Simulation Results." 3GPP document reference R4-070902, 3GPP, Orlando, USA, June 2007. 3GPP TSG-RAN WG4 Meeting 43bis.

[Nor07] Nortel, Vodafone. "Open and Closed Access for Home NodeBs." 3GPP document reference R4-071231, 3GPP, Athens, Greece, August 2007. 3GPP TSG-RAN WG4 Meeting 44.

[Ora07] Orange. "Home BTS consideration and deployment scenarios for UMTS." 3GPP document reference R4-070825, 3GPP, Kobe, Japan, May 2007. 3GPP TSG RAN WG4 Meeting 43.

[Rel] "Overview of 3GPP Release 9 V0.0.6 (2009-06).".

[Spea] "3GPP TS Base Station (BS) radio transmission and reception (FDD) 25.104 V7.7.0 (2007-06).".

[Speb] "3GPP TS Multiplexing and channel coding 25.212 V7.5.0 (2007-05).".

[SWM08] Aimin Sang, Xiaodong Wang, Mohammad Madihian, and Richard D. Gitlin. "Coordinated Load Balancing, Handoff/Cell-Site Selection, and Scheduling in Multi-Cell Packet Data Systems." *Wireless Networks*, **14**(1):103–120, February 2008.

[TGS94] V. S. Tanaev, V. S. Gordon, and Y. M. Shafransky. *Scheduling Theory. Single-Stage Systems.* Kluwer Academic Publishers, Norwell, MA, 1994.

[TR2] "3GPP TR25.8200 V1.0.0 Release 8 (11-2007).".

[WOE05] Christian Wengerter, Jan Ohlhorst, and Alexander Golitschek Edler von Elbwart. "Fairness and Throughput Analysis for Generalized Proportional Fair Frequency Scheduling in OFDMA." *IEEE Trans. on Veh. Technol.*, **3**:1903–1907, May/June 2005.